Research Square

Preprints are preliminary reports that have not undergone peer review.
They should not be considered conclusive, used to inform clinical practice,
or referenced by the media as validated information.

Deep-time geographic dynamics of climate shape global vascular plant diversity

Jiaze Li

jiaze.li19@imperial.ac.uk

Imperial College London https://orcid.org/0000-0003-0247-363X

Iain Prentice

Imperial College London https://orcid.org/0000-0002-1296-6764

Biological Sciences - Article

Keywords:

Posted Date: January 8th, 2026

DOI: https://doi.org/10.21203/rs.3.rs-8229707/v1

License: This work is licensed under a Creative Commons Attribution 4.0 International License.
Read Full License

Additional Declarations: There is **NO** Competing Interest.

Deep-time geographic dynamics of climate shape global vascular plant diversity

Jiaze Li[1], Iain Colin Prentice[1,2]

[1]*Georgina Mace Centre for the Living Planet, Department of Life Sciences, Imperial College London, Silwood Park Campus, Buckhurst Road, Ascot, SL5 7PY, UK*

[2]*Department of Earth System Science, Ministry of Education Key Laboratory for Earth System Modeling, Institute for Global Change Studies, Tsinghua University, Beijing 100084, China*

Corresponding author: Jiaze Li (email: jiaze.li19@imperial.ac.uk)

Abstract

Climate has been proposed to shape global biodiversity through multiple, competing mechanisms that emphasise either magnitude, spatial distribution, or temporal stability of climatic variables[1–4], without integrating these dimensions into a unified spatio-temporal framework. Here we quantify spatio-temporal climate change in both climatic and geographic spaces by tracing when and where climatic conditions have emerged, persisted, and shifted across the Earth's surface over the past 50 million years. We compile the most comprehensive global vascular plant diversity map to date (350,864 species) to test how deep-time geographic dynamics of climate have influenced plant diversity patterns. We find that species-rich and evolutionarily diverse plant communities are associated with climates that originated early, remained geographically extensive over long time, and experienced moderate geographic shifts. These climates are primarily warm and humid, now dominant in the tropics but previously extending into high latitudes. Models incorporating climate and its deep-time geographic dynamics explain up to 95% of the global variation in plant diversity, with geographic extent and mobility of climate contributing over half the explanatory power for species richness, turnover, and phylogenetic diversity. This work addresses a fundamental question

that has long been debated regarding the spatio-temporal impacts of ongoing climate change on biodiversity.

Main

That warm, humid tropical regions harbour more species than cold, dry higher latitudes is one of the fundamental patterns of life on Earth[1,2,4–6]. It is accepted that climate plays a key role in shaping global biodiversity patterns by affecting the speciation, dispersal, and extinction[7–11] of animals[12,13], plants[14,15], and microbes[16]. However, the underlying mechanisms remain the subject of ongoing debate[1,17,18].

A well-studied explanation for how climate shapes latitudinal biodiversity gradient is the 'species-energy hypothesis', which posits that environments with greater energy and water availability (e.g., temperature, precipitation, and productivity) support more species[19–23]. Yet, accumulating evidence suggests that the geography and history of climate may be of equal or greater importance than any intrinsic property of climate[3,4]. The importance of climate geography was first formalized in the 'area hypothesis', stating that larger area of tropics provides greater carrying capacity for higher species richness[24–26]. More recently, this idea was refined into the 'area-isolation hypothesis' by Coelho and colleagues[13]. They further incorporated the geographic isolation of a climate – measured as the average distance among disconnected fragments of the same climate – as a driver of speciation[13]. In parallel, other hypotheses focus on the climate history of locations. The 'evolutionary-time hypothesis' argues that the tropics, being older than higher latitudes, have hosted lineages that originated in tropical climates for longer, allowing more time for diversification and species accumulation[17,27–29]. The 'stability hypothesis' proposes that the tropics, having been less affected by past glaciations and large-scale climatic disruptions, offered lineages relatively continuous opportunities for diversification, whereas higher latitudes experienced repeated extinctions and recolonisation[12,18,30,31].

None of these hypotheses simultaneously considers the dual dynamics of climate in space and time. Hypotheses focused on climate geography are temporally static. They explain current biodiversity patterns using present-day geographic attributes of climate (e.g., area and isolation) but

ignore how these attributes evolved over millions of years[3,13]. A climatic condition that is widespread today may have experienced contraction and fragmentation in the past[32]. Conversely, hypotheses focused on climate history are spatially static. They measure value changes of climatic variables at fixed locations (e.g., within latitudinal bands), ignoring the key fact that species can track migrating climates suitable for their survival[33]. A climatic condition, defined by a stable set of climatic variables, can persist through time, though its geographic position may shift across the Earth's surface[32]. The limitations of hypotheses based on the geography or history of climate are complementary and together reveal a unifying perspective: the spatio-temporal dynamics of climate may be a primary driver of global biodiversity patterns. From this perspective, climates that remained geographically widespread over long timescales can provide larger and more stable evolutionary stages for persistence, diversification, and accumulation of species[3,4,34]. Simultaneously, geographic expansion, contraction, and migration of climate over evolutionary time are expected to influence species dispersal, extinction, and speciation[32,33]. However, how the deep-time geographic dynamics of climate have shaped global biodiversity patterns remain unknown.

Quantifying the spatio-temporal influence of climate on global biodiversity requires a shift in analytical framework – from geographic to climatic space. This can be achieved by constructing a multi-dimensional space using climatic variables, which is then discretised into a grid of 'climatic bins', each representing a unique climatic condition[3,13]. One climatic bin may span disconnected geographic regions across both present and past, enabling the identification of historical geographic distributions and the quantification of spatio-temporal dynamics for each climatic condition. Within this framework, vascular plants are central. As primary producers constituting over 80% of Earth's biomass, vascular plants form the structural and trophic foundation of terrestrial ecosystems[35]. Variation in plant diversity can influence the composition and diversity of other terrestrial trophic levels[36–38]. Fossil pollen and macrofossil records also demonstrate that plants can track climate change via continental-scale migration[33,39].

A further challenge lies in defining an appropriate timescale. Phylogenomics of angiosperms reveals an early burst of diversification during the Late Jurassic and Early Cretaceous, which gave rise to more than 80% of extant angiosperm orders[40]. This was followed by a long period of steady,

slower diversification for at least 80 million years through the remaining Mesozoic, during which around three-quarters of all modern angiosperm families originated[40]. A second surge in diversification rates occurred in the Cenozoic, concurrent with a period of global cooling that may have acted as a driver for this resurgence[40]. From the Early Eocene to the Late Pliocene (*ca*. 55–2.6 Ma), long-term cooling eliminated high-latitude tropical climates and expanded temperate climates poleward, contributing to the modern latitudinal diversity gradient[32]. The subsequent Quaternary was marked by glacial-interglacial cycles with large fluctuations in temperature, precipitation, and CO_2 concentration, imposing strong environmental filtering on species[33]. The Holocene and the pre- and post-industrial periods reflect post-glacial warming and the increasing impact of human activities[41].

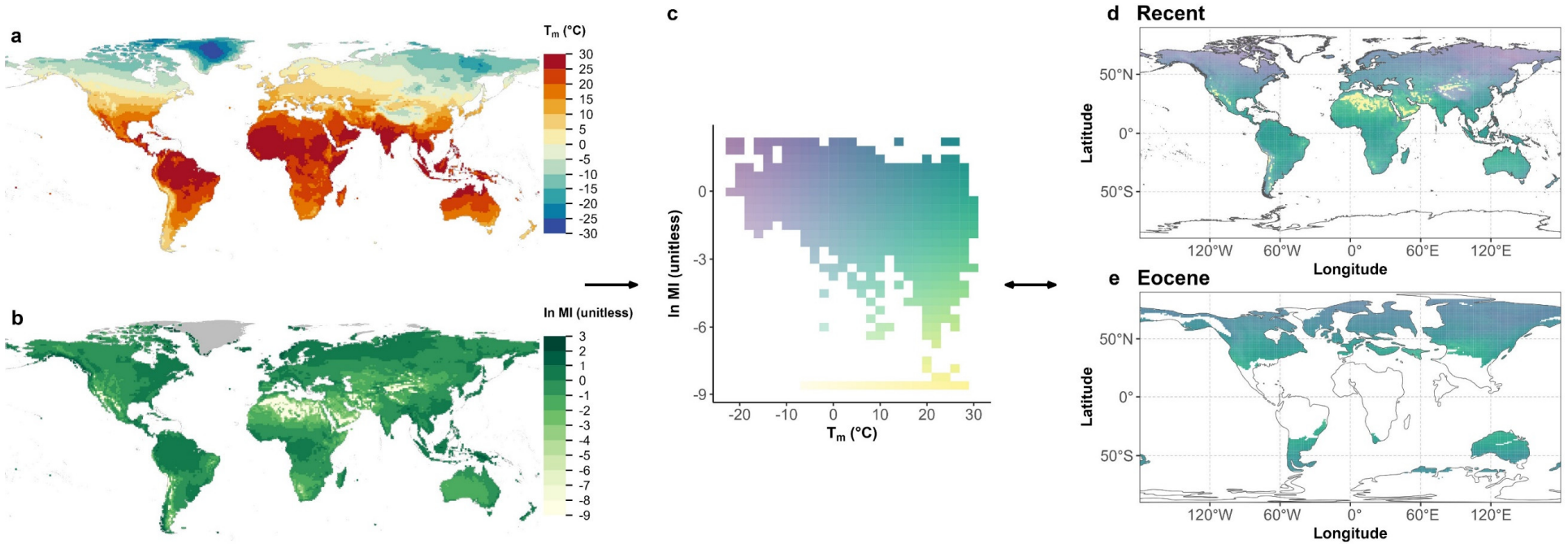
Here, we investigated how climate and its deep-time geographic dynamics have shaped present-day global patterns of vascular plant diversity. We hypothesised that (1) climates that have remained widespread over evolutionary time harbour more species, and (2) the historical stability of climate' geographic extent influences species composition. By compiling global occurrence records for 350,864 vascular plant species, we generated the most comprehensive data-based map of global plant diversity to date. We defined a climatic space based on recent (1901–1989) temperature and plant-available moisture data. Within this space, analogues of each climatic condition were identified across key geological periods for which multiple palaeoclimate model simulations are available: the Eocene (*ca*. 50 Ma), Mid-Pliocene (3.3–3.0 Ma), Last Glacial Maximum (LGM, 22–18 ka), Mid-Holocene (*ca*. 6 ka), and pre-industrial (pre-1850) periods. We quantified the geographic extent of climatic conditions, as well as their persistence and shift, across the selected periods. Finally, we assessed the relative contributions of contemporary climate and its deep-time geographic dynamics in explaining global vascular plant diversity today.

Historical geography of contemporary climates

A temperature index (T_m, °C) and a log-transformed moisture index (ln MI, unitless) were used to define a two-dimensional climatic space (Fig. 1a–c). These two bioclimatic variables represent major independent climatic controls on the global geographic distribution of plants[42–45], with T_m capturing the latitudinal temperature gradient[46] and ln MI representing plant-available moisture[42–45]

(see Methods). The climatic space was constructed using climate data from 1901 to 1989, a recent period selected to reflect post-industrial conditions prior to the onset of accelerated anthropogenic influence around 1990[47]. Multiple grid resolutions of the climatic space were generated by dividing each axis into equal intervals (see Methods); all main-text results are based on the 30-interval resolution, with results from alternative resolutions (40, 50, and 60 intervals) reported in the Supplementary Information. Each grid cell in the climatic space – hereafter referred to as a 'climatic bin' – represents a distinct recent climatic condition[3,13,48] and is visualised by a unique colour (Fig. 1c, and see Figs. S1 and S2 for alternative colour gradient schemes). Each bin may correspond to multiple geographic locations across different time periods[3,13,48]. This property allows for the tracing of the historical geography of recent climatic conditions. We then identified the geographic locations of these climatic conditions in the recent period (1901–1989, Fig. 1d) and in five geohistorical periods (Extended Data Fig. 1).

Fig. 1: Mapping climates in geographic and climatic spaces.



a and **b**, Geographic distributions of the two bioclimatic variables used to define the climatic space: the temperature index (**a**, T_m, °C) and the natural-log-transformed moisture index (**b**, ln MI, unitless), for the recent reference period (1901–1989). **c**, The two-dimensional climatic space defined by the recent T_m and ln MI, partitioned into 30 equal intervals along each axis. Each coloured grid cell ('climatic bin') represents a unique climatic condition (405 cells in total). Alternative colour gradient schemes are provided in Figs. S1 and S2. **d** and **e**, The application of the framework to trace historical geography of recent climates. The map in **d** shows the geographic locations of all climatic bins during the recent period (1901–1989). The map in **e** shows the geographic locations where those same climatic conditions (defined in **c**) existed during the Eocene (*ca.* 50 Ma); uncoloured areas

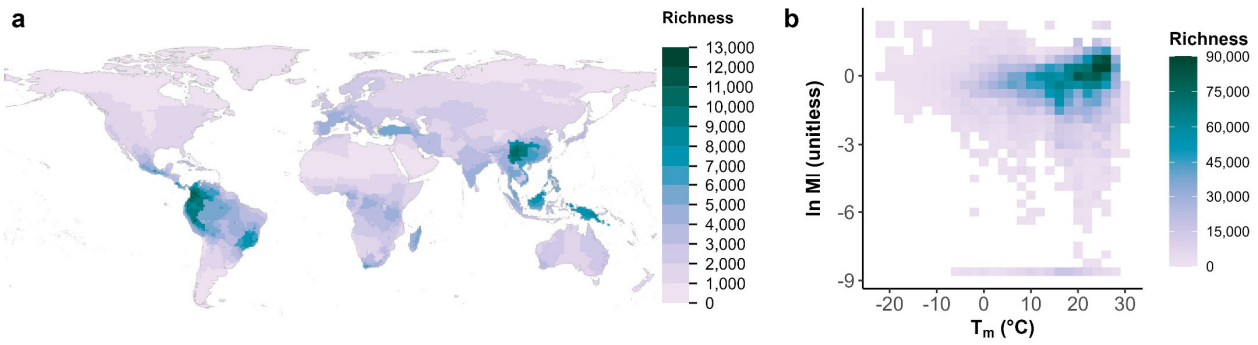
denote climatic conditions absent during this period. Colours correspond to those in **c**, with identical colours indicating the same climatic conditions. The same colour gradient scheme is consistently applied across subsequent figures. The geographic distribution of recent climatic conditions in other geological periods is shown in Extended Data Fig. 1. All maps are shown at a 1° spatial resolution.

Global patterns of vascular plant diversity

By compiling native occurrence records for 350,864 vascular plant species (see Methods), representing over 98% of accepted species in the World Checklist of Vascular Plants (WCVP)[49], we generated a data-based global map of plant species richness at 1° spatial resolution (Fig. 2a, see Methods for details). To map plant diversity patterns in climatic space, we counted the number of species occurring within each climatic bin defined by T_m and ln MI (Fig. 2b). While global patterns of plant diversity have previously been explored through model-based or empirical approaches[14,49–55], our map represents the most taxonomically complete global dataset compiled to date at fine spatial resolution (Table S1).

Hotspots of plant diversity (Figs. 2a and S3) are concentrated in Central and South America, including the Andes-Amazonia and Atlantic Forest in Brazil; in the mountains of Southwest China; across Southeast Asia, extending from the Indochina and Malay Archipelago to the island of New Guinea; in parts of Africa, encompassing Cameroon, Tanzania, Madagascar and the Cape region of South Africa; and in parts of Europe and West Asia including the Alps, the Mediterranean basin and the Caucasus mixed forests. In climatic space (Fig. 2b), species richness peaks under warm conditions ($T_m \approx 19–28$ °C) and humid conditions (MI > 1). These patterns are consistent with previous estimates[14,49–56].

Fig. 2: Global patterns of vascular plant diversity across geographic and climatic spaces.



a, Global species richness map for vascular plants at 1° spatial resolution, based on native distributions derived from occurrence records of 350,864 species. **b**, Global patterns of vascular

plant species richness in the climatic space defined in **Fig. 1**. T_m (°C), recent (1901–1989) temperature index; ln MI (unitless), recent natural-log-transformed moisture index.

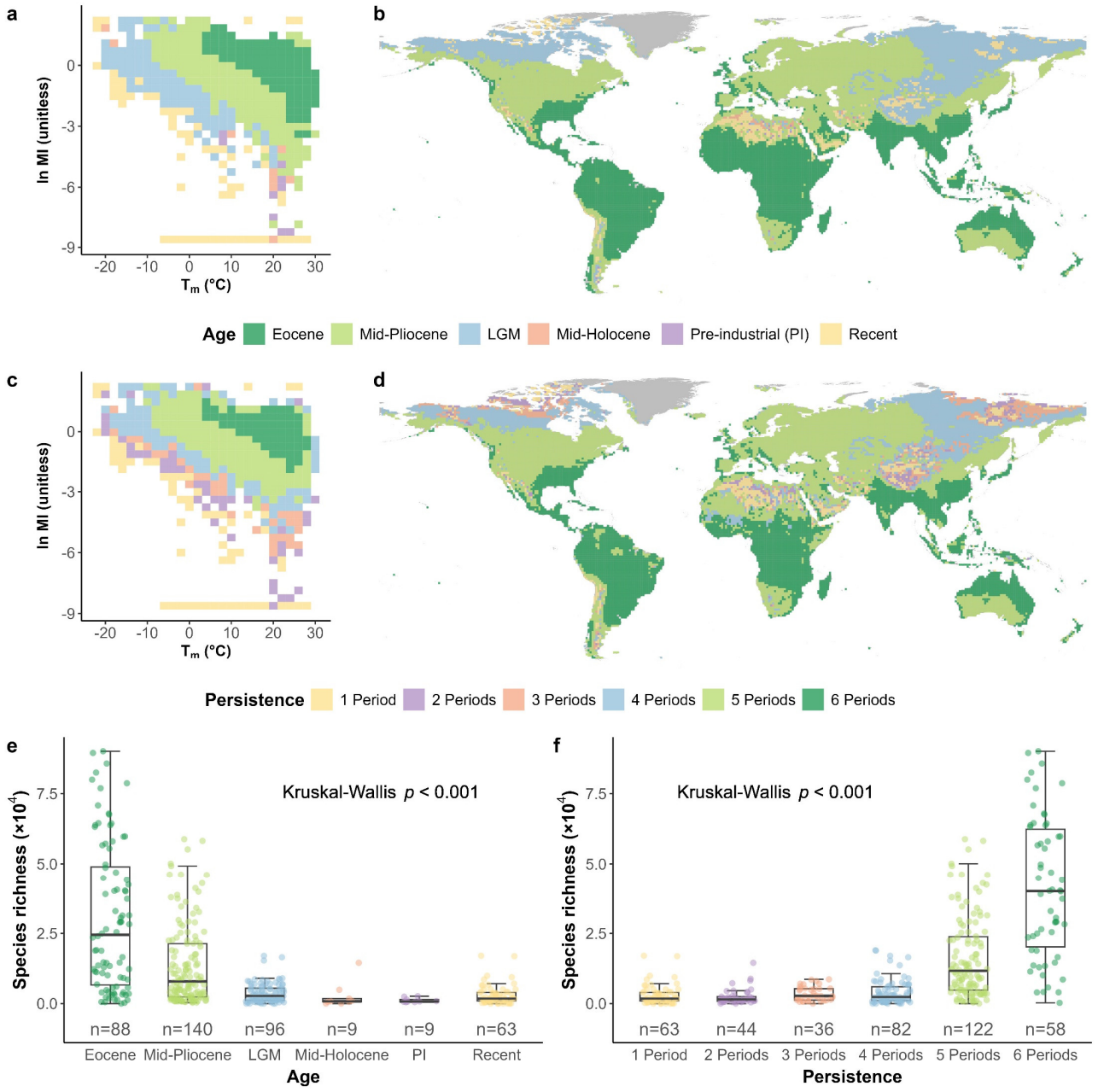
Old and persistent climates harbour more plant species

We evaluated how the age and persistence of recent climatic conditions relate to contemporary plant diversity. 'Age' was defined as the earliest of six selected geological periods during which a recent climatic condition first appeared. 'Persistence' was calculated as the number of these periods in which a climatic condition occurred.

Age and Persistence of recent climates show similar distribution patterns across both climatic and geographic spaces (Fig. 3a–d). Warm and humid climates tend to be both older and more persistent, originating as early as (or before) the Eocene and persisting to the present (Fig. 3a, c). These climatic conditions are predominantly found in present-day tropical regions (Fig. 3b, d). As the Earth cooled from the Eocene to the Pliocene[32], climatic conditions typical of today's temperate zones began to emerge, with many first appearing in the Mid-Pliocene and continuing through to the present (Fig. 3b, d). In contrast, cold and dry climates (Fig. 3a, c) near the poles (Fig. 3b, d) originated more recently, commonly first appearing during Quaternary glacial periods as illustrated by the LGM. Hot and arid climates (Fig. 3a, c) in equatorial regions (Fig. 3b, d) – such as the Sahara, Arabian Peninsula, and Mongolian Plateau – emerged recently.

To assess how the age and persistence of recent climates have influenced recent species richness, we compared richness across climatic bins grouped by Age and Persistence. Species richness varies significantly with both factors ($p < 0.001$ in Fig. 3e–f). Climates with older origins, especially those dating back to the Eocene (median $\approx 2.5 \times 10^4$, $p < 0.001$ in Fig. 3e), and climates that persisted through all six periods (median $\approx 4 \times 10^4$, $p < 0.001$ in Fig. 3f), harbour substantially larger numbers of vascular plant species.

Fig. 3: Age and persistence of climate and their associations with recent species richness.



a and **b**, Age of recent climatic conditions mapped in climatic (**a**) and geographic (**b**) spaces, indicating when each climatic bin first emerged across the six selected geological periods (Eocene to recent). **c** and **d**, Persistence of climates, defined as the number of periods in which a recent climatic condition was present, shown in climatic (**c**) and geographic (**d**) spaces. **e** and **f**, Relationships between plant species richness and Age (**e**) or Persistence (**f**) of climatic conditions were assessed using Kruskal-Wallis tests. Horizontal lines and boxes indicate medians and

interquartile ranges. Sample sizes per group are shown below the boxes. T_m (°C), recent (1901–1989) temperature index; ln MI (unitless), recent natural-log-transformed moisture index.

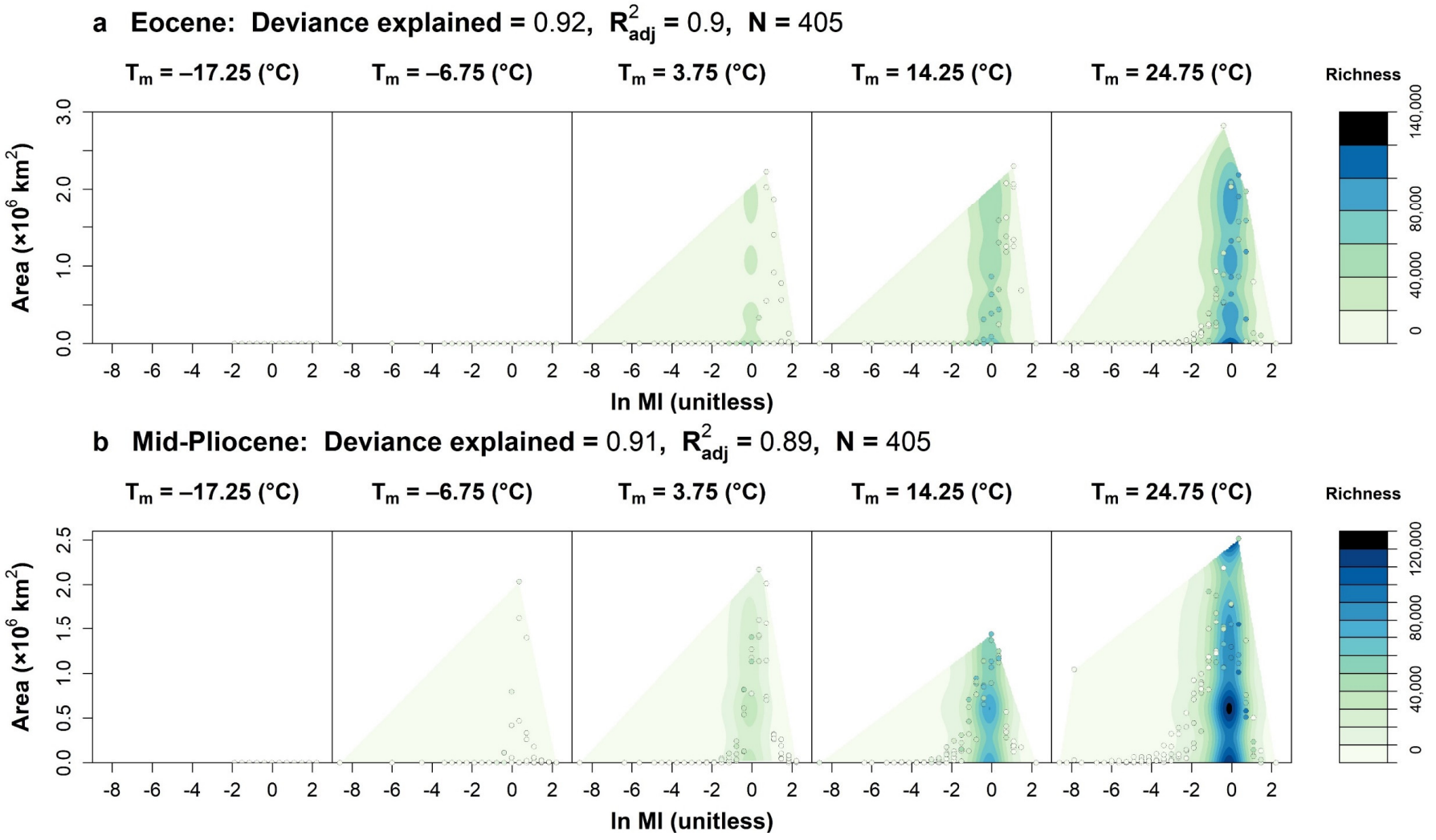
Persistently widespread climates support higher plant species richness

To assess how the geographic extent of climatic conditions influences species richness, we quantified the total land area occupied by each recent climatic condition during five geohistorical periods and the recent period (1901–1989), referred to as 'Area' (km^2). We also calculated the mean 'Area' since the first appearance of each climatic condition, representing its long-term spatial persistence.

We fitted Generalised Additive Models (GAMs) to model species richness in climatic bins as a function of three explanatory variables: two bioclimatic variables (T_m and ln MI) and Area (either from individual periods or averaged across periods). Separate GAMs were fitted for each of the six periods and for mean Area. Across all models, the explanatory variables explain over 90% of the deviance in species richness (Fig. 4 and Tables S3–S9).

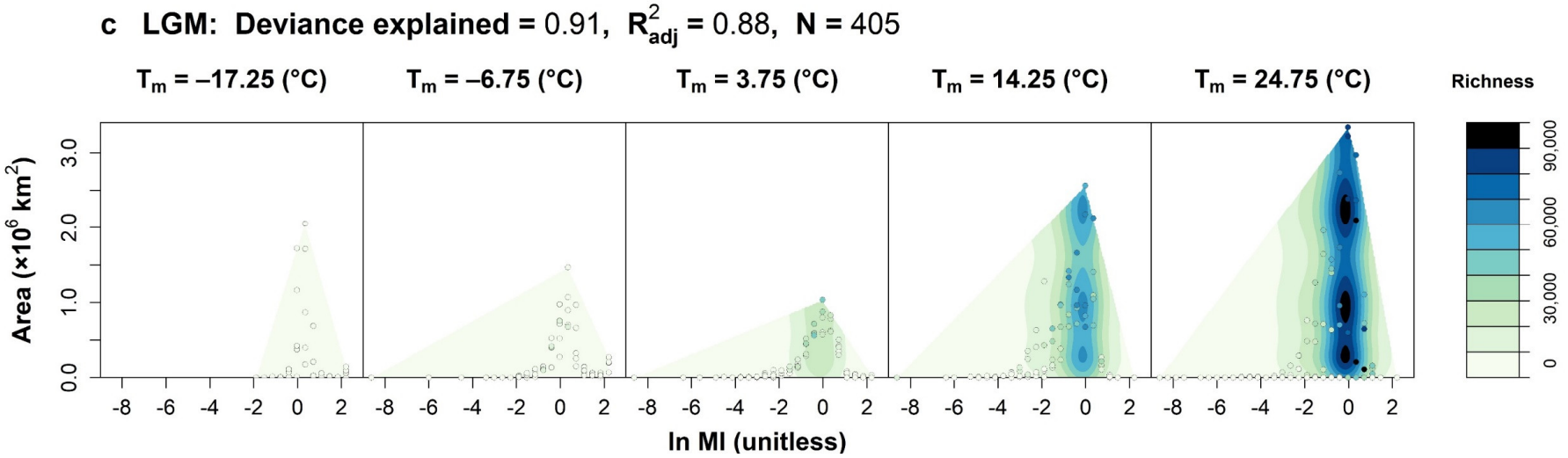
We visualised the relationships between species richness and the three explanatory variables using contour plots (Fig. 4). Across all periods, species richness consistently peaks under warm and humid climatic conditions (T_m = 24.75 °C; MI = 1). However, species richness shows different relationships with Area across periods (Fig. 4). During the Eocene (Fig. 4a), Mid-Pliocene (Fig. 4b), and LGM (Fig. 4c), species richness was relatively insensitive to the geographic extent of climate. From the Mid-Holocene onwards (Fig. 4d–f), species richness was higher in climatic bins occupying larger geographic areas (Area ≥ 3.0×10^6 km^2 in Fig. 4d–f). This pattern is also evident for mean Area across periods (Area ≥ 2.0×10^6 km^2 in Fig. 4g). These results suggest that the long-term persistence of large geographic area, rather than initial spatial extent at the time of emergence, is more important in shaping contemporary plant diversity. Combined with the findings on climate age and persistence (Fig. 3), these results indicate that warm, moist climates that have remained geographically extensive for longer periods tend to support more diverse plant communities.

209 **Fig. 4: Relationships between recent plant species richness and three explanatory variables across selected geological periods.**

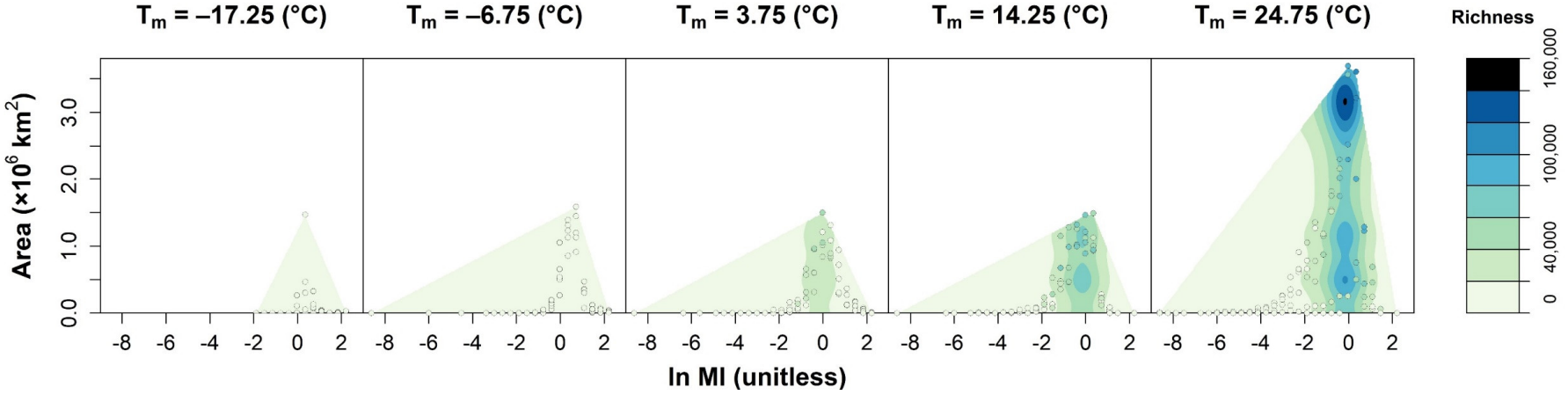


210

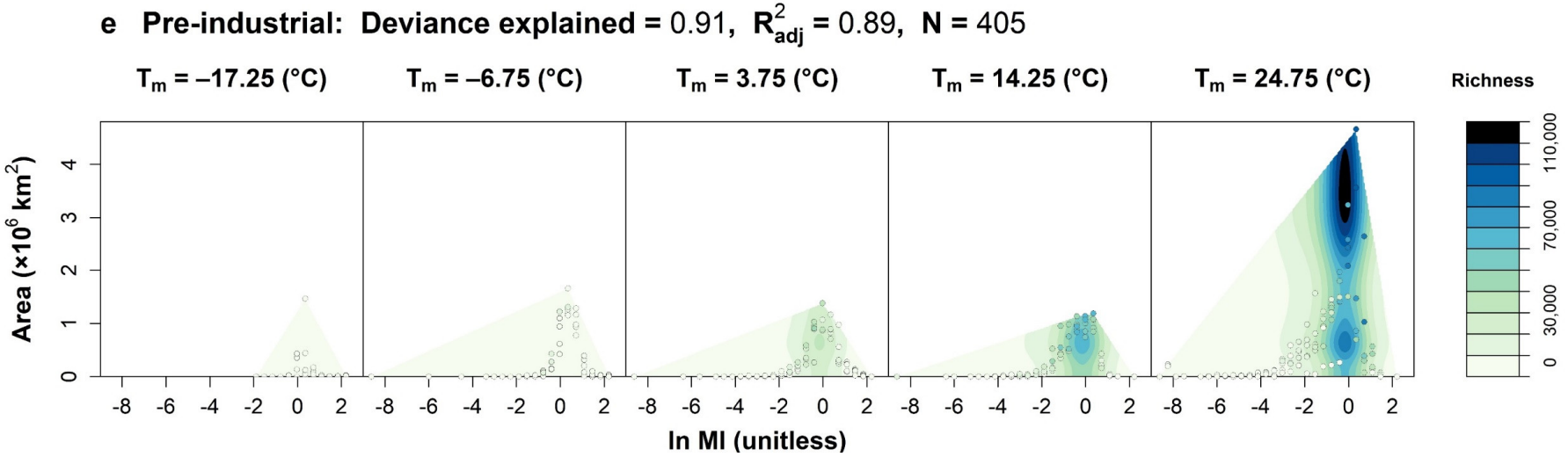
211


c LGM: Deviance explained = 0.91, R^2_{adj} = 0.88, N = 405
T_m = –17.25 (°C)
T_m = –6.75 (°C)
T_m = 3.75 (°C)
T_m = 14.25 (°C)
T_m = 24.75 (°C)
Richness
0
30,000
60,000
90,000
Area (×10^6 km^2)
0.0
1.0
2.0
3.0
-8 -6 -4 -2 0 2
ln MI (unitless)

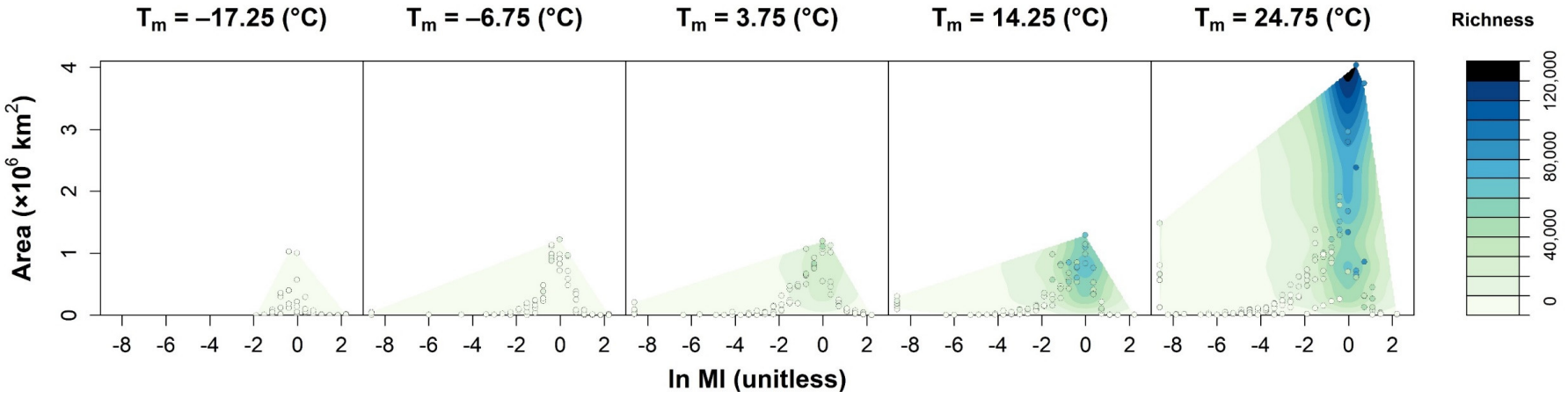
212


d Mid-Holocene: Deviance explained = 0.91, R^2_{adj} = 0.9, N = 405
T_m = –17.25 (°C)
T_m = –6.75 (°C)
T_m = 3.75 (°C)
T_m = 14.25 (°C)
T_m = 24.75 (°C)
Richness
0
40,000
100,000
160,000
Area (×10^6 km^2)
0.0
1.0
2.0
3.0
-8 -6 -4 -2 0 2
ln MI (unitless)

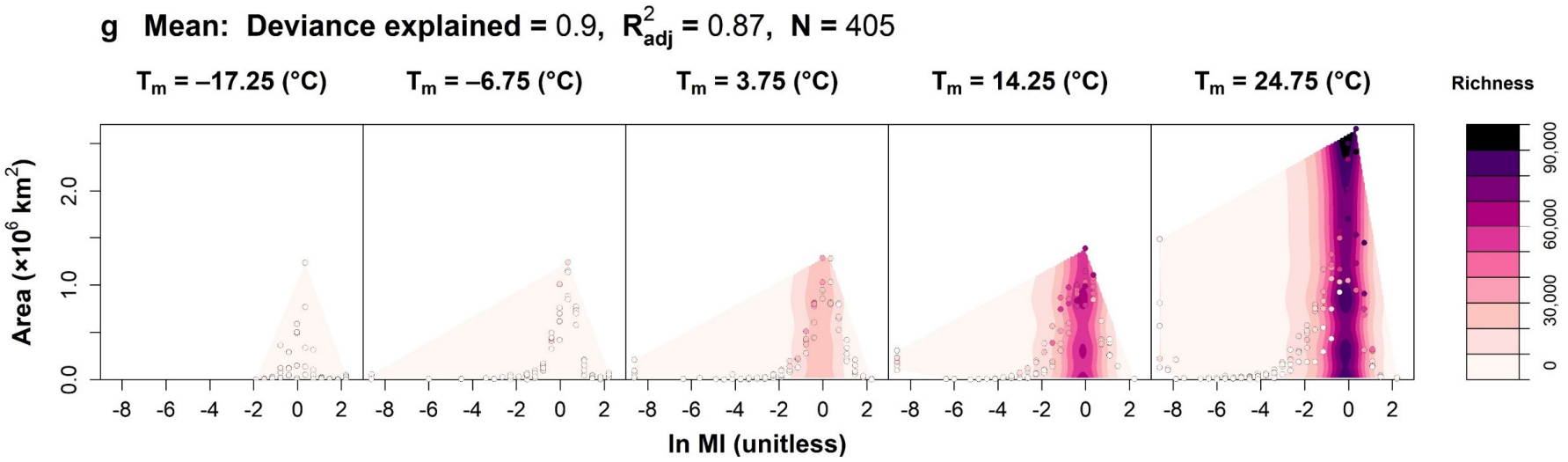
213


e Pre-industrial: Deviance explained = 0.91, R^2_{adj} = 0.89, N = 405
T_m = –17.25 (°C)
T_m = –6.75 (°C)
T_m = 3.75 (°C)
T_m = 14.25 (°C)
T_m = 24.75 (°C)
Richness
Area (×10^6 km^2)
ln MI (unitless)

214


f Recent: Deviance explained = 0.93, R^2_{adj} = 0.94, N = 405
T_m = –17.25 (°C)
T_m = –6.75 (°C)
T_m = 3.75 (°C)
T_m = 14.25 (°C)
T_m = 24.75 (°C)
Richness
Area (×10^6 km^2)
ln MI (unitless)

215



Contour plots show fitted species richness from Generalised Additive Models (GAMs), with species richness modelled as a function of T_m, ln MI, and Area. Panels correspond to: **a**, Eocene (*ca.* 50 Ma); **b**, Mid-Pliocene (3.3–3.0 Ma); **c**, Last Glacial Maximum (LGM, 22–18 ka); **d**, Mid-Holocene (*ca.* 6 ka); **e**, pre-industrial period (pre-1850); **f**, recent period (1901–1989); and **g**, mean Area since the first appearance of each climatic condition across all selected geological periods. Fitted species richness values are shown as contour levels; observed species richness values are overlaid as dots. Darker colours on the right corresponding scale bar indicating higher species richness. Values of ln MI and Area vary continuously along the horizontal and vertical axes, respectively, with each slice created at a specific T_m value. T_m (°C), recent (1901–1989) temperature index; ln MI (unitless), recent natural-log-transformed moisture index; Area (km^2), total land surface area occupied by each climatic condition during the corresponding geological period.

Moderate climatic shifts promote plant diversity

A climatic condition that has occupied different geographic locations through time, and its expansion, contraction, or migration, may influence plant community composition. To quantify these dynamics, we developed two metrics. First, we calculated the change in total land area occupied by each climatic condition between its earliest occurrence (among six selected periods) and the recent period, denoted as 'ΔArea' (km^2). Positive values indicate spatial expansion, while negative values indicate contraction. Second, we measured the geographic shift of each climatic condition using the average great-circle distance between its initial and recent geographic distributions, termed 'Movement' (km). In addition to species richness, we computed three more diversity metrics within climatic bins. We measured species turnover among geographic grid cells sharing the same climatic condition, indicating how species composition varies geographically under constant climate. We also calculated Faith's phylogenetic diversity (PD, Ma)[57], representing the total evolutionary history accumulated within each climatic bin. Given the strong dependence of PD on species richness, we also derived relative phylogenetic diversity (RPD, Ma) by regressing PD on richness and extracting the residuals. Large positive RPD values indicate species in a climatic bin are more distantly related than expected, while negative values suggest phylogenetic clustering.

We fitted GAMs to examine how each diversity metric responds to five explanatory variables: two bioclimatic variables (T_m and ln MI), Area, ΔArea, and Movement. Area was drawn from the recent period, as it served as the reference point for calculating ΔArea. Pairwise correlations among these explanatory variables are low, reducing concerns of concurvity (Fig. S12). The GAMs explain 95% of the deviance in species richness ($R_{pred}^2 = 0.95$, $R_{adj}^2 = 0.95$), 74% of the deviance in species turnover ($R_{pred}^2 = 0.77$, $R_{adj}^2 = 0.75$), 85% of the deviance in PD ($R_{pred}^2 = 0.85$, $R_{adj}^2 = 0.84$) and 53% of the deviance in RPD ($R_{pred}^2 = 0.53$, $R_{adj}^2 = 0.49$).

We also assessed the effects of climate age and persistence on species turnover, PD, and RPD (Extended Data Fig. 3). Older and more persistent climates tend to support greater species turnover and higher PD ($p < 0.001$ in Extended Data Fig. 3 a–d). Climates that were present as early as the Eocene and persisted to the present harboured more distantly related and/or evolutionarily ancient

253 species (RPD > 0, Extended Data Fig. 3 e–f), whereas those first appearing in the Mid-Pliocene
254 hosted more phylogenetically clustered and/or evolutionarily younger assemblages (RPD < 0,
255 Extended Data Fig. 3 e–f). In contrast, more recently emerged climates showed little phylogenetic
256 structuring (RPD ≈ 0, Extended Data Fig. 3 e–f). Based on these findings, we also fitted separate
257 GAMs for climatic bins grouped by their Age, excluding groups postdating the Mid-Holocene due
258 to small sample sizes.

259 Partial residual plots were generated to visualise the independent relationships between each
260 explanatory variable and species richness (Fig. 5a–e), species turnover (Fig. 5f–j), PD (Fig. 5k–o)
261 and RPD (Fig. 5p–t). Nearly all diversity metrics increase significantly with both temperature and
262 moisture, except turnover, which shows no relationship with ln MI (Fig. 5g). Recent Area is
263 positively correlated with species richness (Fig. 5c), turnover (Fig. 5h), and PD (Fig. 5m), but
264 negatively with RPD (Fig. 5r). These patterns are robust across Age groups (Extended Data Figs. 4,
265 6 and 8).

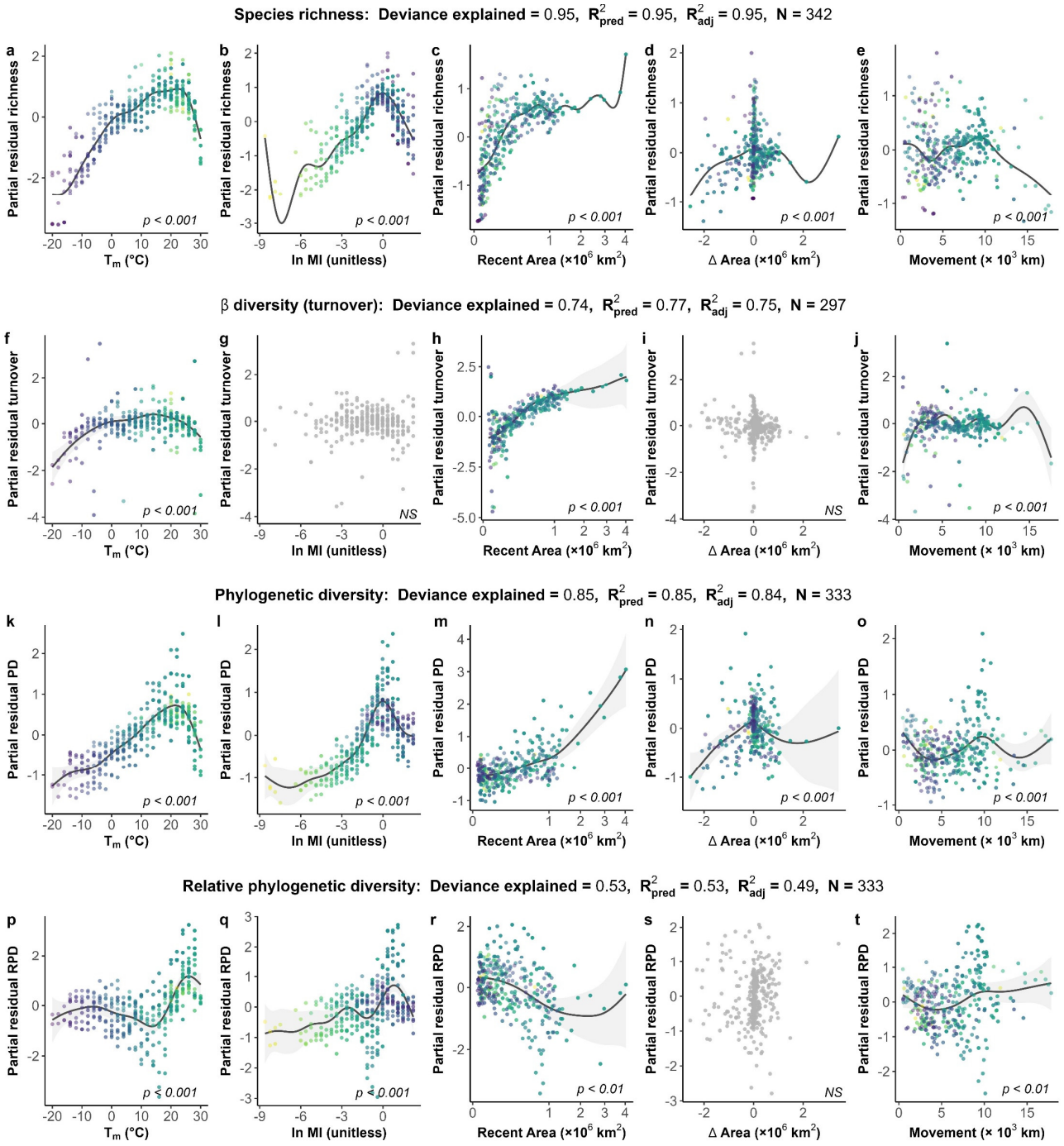
266 Climatic conditions experiencing geographic contraction (i.e. ΔArea < 0) are associated with
267 lower species richness and PD, while geographic expansion (i.e. ΔArea > 0) does not consistently
268 increase diversity (Fig. 5d and n). Instead, peak species richness and PD occur in climates with
269 relatively stable area through time, i.e. with ΔArea close to 0 km^2 (Fig. 5d and n). This pattern
270 suggests that long-term geographic stability, rather than expansion *per se*, has been key to fostering
271 plant diversity.

272 The influence of Movement on plant diversity is more complicated. Moderate geographic shifts
273 (5,000–10,000 km) are associated with higher species richness and PD, whereas both metrics
274 decline when Movement exceeds this range (Fig. 5e and o). These negative effects are largely
275 attributable to the warm, humid climates that occurred at high latitudes during the Eocene but now
276 correspond to tropical regions in the present day (Extended Data Fig. 4e). In contrast, climates
277 originating in the Mid-Pliocene or LGM showed positive associations between Movement and
278 richness when Movement remained below 10,000 km (Extended Data Figs. 6e and 8e). Species
279 turnover increases with Movement up to ~5,000 km, then plateaus (Fig. 5j), particularly evident for
280 climatic conditions that originated during the Mid-Pliocene and LGM (Extended Data Figs. 6j and

8j). RPD shows a weak but statistically significant positive correlation with Movement (Fig. 5t), although this pattern does not persist within Age groups (Extended Data Figs. 4t, 6t and 8t).

We further quantified the relative importance of each explanatory variable in determining plant diversity (Fig. 6). Among the five variables, recent Area and Movement consistently contribute the most explanatory power for species richness, species turnover, and PD, exceeding the combined contribution of the other three predictors. In contrast, RPD is primarily influenced by climatic conditions themselves (T_m and ln MI), while recent Area, ΔArea, and Movement have little effect. This suggests that environmental filtering by present-day climate, rather than historical geographic dynamics of climate, plays a stronger role in shaping phylogenetic structure of plant communities[58].

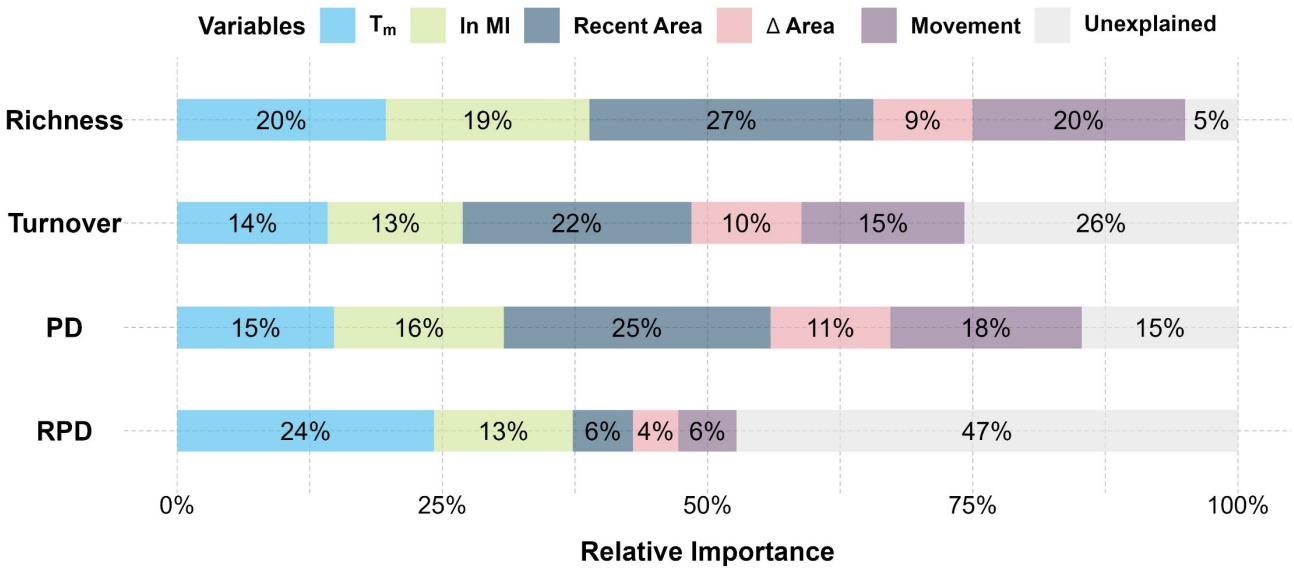
Fig. 5: Influence of climate and its deep-time geographic dynamics on plant diversity.



Partial residual plots from Generalised Additive Models (GAMs) showing the independent relationships between four metrics of vascular plant diversity and five explanatory variables. Rows correspond to the four diversity metrics: species richness (**a**–**e**), species turnover (**f**–**j**), phylogenetic diversity (PD, **k**–**o**), and relative phylogenetic diversity (RPD, **p**–**t**). Columns correspond to the five explanatory variables: T_m (°C), recent (1901–1989) temperature index; ln MI (unitless), recent

natural-log-transformed moisture index; Recent Area (km^2), total land area occupied by a climatic condition in the recent period; ΔArea (km^2), change in total land area occupied by a climatic condition from its earliest occurrence to the recent period; Movement (km), geographic shift of a climatic condition since its earliest occurrence to the recent period. Black lines represent smooth curves of the GAM regression. Shaded areas indicate 95% confidence intervals, which are not visible in some cases due to narrow uncertainty. Each coloured dot represents a climatic bin, coloured by the gradient used in **Fig. 1c–e**. Statistically non-significant terms ($p > 0.05$) are shown as grey dots with no fitted curve. Model performance is reported as deviance explained, predicted R^2 (R_{pred}^2) and adjusted R^2 (R_{adj}^2).

Fig. 6: Relative importance of climate and its deep-time geographic dynamics in explaining plant diversity.



Relative importance of five explanatory variables estimated by partitioning deviance explained by Generalised Additive Models (GAMs). T_m (°C), recent (1901–1989) temperature index; ln MI (unitless), recent natural-log-transformed moisture index; Recent Area (km^2), total land area occupied by a climatic condition in the recent period; ΔArea (km^2), change in total land area occupied by a climatic condition from its earliest occurrence to the recent period; Movement (km), geographic shift of a climatic condition since its earliest occurrence to the recent period. Each stacked bar represents the total deviance in a given diversity metric, with coloured segments

indicating the proportion attributed to each explanatory variable and the grey segment showing unexplained deviance.

Discussion

Contemporary climates that support the highest plant diversity – primarily warm and humid conditions – tend to share four key characteristics: they are ancient, persistent, geographically extensive, and have undergone moderate geographic shifts over time. Many of these climates had already emerged by the Eocene (*ca*. 50 Ma), and although their geographic locations have changed, they have remained present until today and are now mainly found in tropical regions. Climatic conditions that have consistently occupied large geographic areas over long timescales, rather than those that expanded more recently without long-term persistence, support higher species richness, species turnover, and phylogenetic diversity. Moderate geographic shifts have further promoted diversity, whereas extensive movements are associated with diversity loss. Collectively, our results highlight that the early emergence, persistently large spatial extents, and moderate mobility of climatic conditions jointly contribute to the formation and maintenance of rich and evolutionarily diverse plant communities.

Climates that have remained steadily widespread over deep time likely preserve ancient lineages and reduce extinction risks[8,59]. Because many species retain ancestral ecological requirements (niche conservatism), spatially extensive climates that emerged early and persisted longer provide more time for lineages to diversify within their ancestral environments[11]. Such climatic conditions may act as evolutionary 'museums'[8], conserving both species and phylogenetic diversity. In addition, a large geographic extent facilitates species survival under environmental fluctuations by increasing opportunities for migration rather than extinction. Species-area relationships in climatic space may also reflect capacity rules[13]: climates occupying larger areas tend to support larger populations, which are generally associated with lower extinction rates and potentially higher speciation rates[26]. Palaeoclimate events such as glacial-interglacial cycles likely introduced temporal heterogeneity in non-climatic environmental factors such as soils, topography, and hydrology. These changes may have reshaped species compositions within the same climatic

conditions across time through repeated colonisation, niche differentiation, and community reassembly.

Moderate geographic movement of climate can further promote diversification by fragmenting populations and facilitating species dispersal[59]. As climatic conditions shift spatially, populations may become fragmented across regions, creating opportunities for allopatric speciation[60,61]. At the same time, lineages with sufficient dispersal capacity can track their climatic niches and colonise new regions, while those with intermediate levels of adaptive niche evolution may persist or diversify *in situ* under the novel climatic conditions[8]. By contrast, extensive climatic shifts may have negative effects on biodiversity. Movements exceeding species' dispersal capacities or their adaptive niche evolution rates can lead to local extinction or metapopulation collapse[8,62]. For example, warm and humid climates now widespread in the tropics were distributed at high latitudes during the Eocene. The equatorward displacement of these climates, which occurred ~30–40 million years ago, may have contributed to the extinction of some 'tropical' species and clades previously found at higher latitudes[4,32].

While our study reveals how deep-time geographic dynamics of climate have shaped present-day global patterns of plant diversity, it does not incorporate changes in taxonomic richness and floristic composition through time. Fossil records offer valuable information about past floristic diversity and vegetation structure[41,63]. Understanding how the taxonomic composition of past communities under similar climatic conditions differs from that of modern assemblages helps reveal spatio-temporal dynamics of plant diversity. Such comparisons, capturing turnover in community composition between ancient and modern climate analogues, can help identify which climatic conditions have historically functioned as 'cradles' (promoting high speciation), 'museums' (preserving ancient lineages), or 'graves' (marking high extinction) of plant diversity[8,59]. Moreover, current global-scale palaeoclimate reconstructions remain limited by spatial resolution. At the global scale, deep-time climate change was accompanied by major Earth system processes such as continental drift and mountain uplift, both of which are recognised as important drivers of biodiversity patterns[64,65]. However, the effects of these interacting processes are often obscured at coarse spatial resolutions. As high-resolution palaeoclimate reconstructions become increasingly available, future research could investigate the geographic dynamics of climate along elevational

gradients. Such exploration may clarify how interactions between climate change and topographic development have shaped montane biodiversity. Nevertheless, our study presents a framework for integrating the spatial and temporal dimensions of climate dynamics: moving beyond conventional assessments of climatic variable variability in geographic space, to a climate-space approach that quantifies the geographic distribution of climatic conditions and their emergence, persistence and movement over millions of years.

Today, biodiversity loss and climate change are increasingly recognised as 'inseparable challenges' facing our planet[66]. The 16th United Nations Biodiversity Conference of the Parties (COP16) in 2024 reaffirmed the urgency of aligning biodiversity conservation with climate action[67]. Our findings contribute to this goal by identifying the deep-time geographic attributes of climate that are critical for plant diversity conservation, thereby informing implementation of the Kunming-Montreal Global Biodiversity Framework (Targets 1–3, 8 and 21) and the new Global Strategy for Plant Conservation[67,68]. Climates that have remained widespread over deep time represent long-term reservoirs of biodiversity, offering valuable opportunities for restoring and conserving native vegetation. Conservation efforts should also account for both the diversification potential and extinction risks associated with ongoing geographic shifts of climate. Effective conservation must therefore move beyond a static, location-based framework by integrating the spatio-temporal dynamics of climate – tracking the emergence, persistence, extent, and movement of climatic conditions over time – as essential indicators for biodiversity monitoring and planning in a changing world[69].

Methods

Bioclimatic variables

Two bioclimatic variables were selected for this research: a temperature index (T_m, °C), calculated as the average of mean temperature of the coldest month (MTCO, °C) and the warmest month (MTWA, °C); and a moisture index (MI, unitless), derived from the ratio of mean annual precipitation (MAP, mm) to the mean annual potential evapotranspiration (PET, mm). The natural-log transformed MI (ln MI) was used in the analysis to emphasise differences at the dry end

of the moisture range[45]. The variables correspond to the two recognised climatic dimensions that regulate the global geographic distribution of plants[42–45], with T_m reflecting the latitudinal gradient of temperature[46] and MI (ln MI) representing plant-available moisture[42–45].

We selected six representative geological periods across the Cenozoic Era: the Eocene (*ca.* 50 Ma), Mid-Pliocene (3.3–3.0 Ma), Last Glacial Maximum (LGM, 22–18 ka), Mid-Holocene (*ca.* 6 ka), pre-industrial period (pre-1850), and a recent period from 1901 to 1989. For each of these periods, the two bioclimatic variables (T_m and ln MI) were calculated based on climatological data of four raw climatic variables: monthly averaged mean daily air temperature (*tas*, °C), mean monthly precipitation (*pr*, mm), monthly accumulated surface downwelling shortwave radiation (*rsds*, W m^{-2}), and elevation (*elev*, m).

We collected the required gridded climate data from various databases for the selected periods (Table S2). Climatological simulations of the four raw climatic variables in the Eocene were collected from the Deep-Time Model Intercomparison Project (DeepMIP version 1.0; http://www.deepmip.org)[70]. For the Mid-Pliocene, LGM and Mid-Holocene, simulations of the four variables were derived from ensemble model under the Paleoclimate Modelling Intercomparison Project Phase 4 (PMIP4; https://pmip.lsce.ipsl.fr/)[71]. Pre-industrial simulations of the four raw climatic variables were obtained from the Coupled Model Intercomparison Project Phase 6 (CMIP6)[72]. For the recent period (1901–1989): *tas* and *pr* data were downloaded from the Climatic Research Unit (CRU) Time-Series (TS) database (version 4.09: https://catalogue.ceda.ac.uk/uuid/9cf07e92afaa405da4f40b6733f362d3)[73]; *elev* data derived from the SRTM elevation data was acquired from WorldClim v.2.1 (https://www.worldclim.org/)[74]; *rsds* data were obtained from CMIP6[72].

We retained the climate model simulations that have shown strong agreement with available observations or proxy-based climate reconstructions for each selected geological period (Table S2). The multi-model ensemble mean of these selected simulations was then calculated for the four climatic variables to represent the climatology of each period. Detailed descriptions of the paleoclimate simulations and climate databases used are provided in Table S2. We utilised vector maps of land boundaries for the Eocene and Mid-Pliocene epochs from Knowing Earth (http://www.knowing.earth)[75] and raster map of land boundary for other periods from Natural Earth

(https://www.naturalearthdata.com) to derive global land-surface climate data. All gridded climate data were aggregated and reprojected to a spatial resolution of 1° using bilinear interpolation, implemented via the 'projectRaster()' function in the *raster* R package[76] for further calculations.

We applied the Simple Process-Led Algorithms for Simulating Habitats (SPLASH) model with the above-mentioned four climatic variables as inputs to calculate the mean monthly potential evapotranspiration (PET, mm) using the 'splash.grid()' function in the R package *rsplash*[77,78]. The two bioclimatic variables – T_m and ln MI – for all geological periods were then calculated as follows:

$$T_m\ (℃) = \frac{\underset{1\le k\le 12}{min}\ tas_k + \underset{1\le k\le 12}{\max}\ tas_k}{2} \quad (1)$$

$$MI\ (\text{unitless}) = \frac{\sum_{k=1}^{12} pr_k}{\sum_{k=1}^{12} PET_k} \quad (2)$$

where tas_k (°C) is monthly average temperature; pr_k (mm) is mean monthly precipitation; PET_k (mm) is mean monthly potential evapotranspiration calculated from the SPLASH model using *tas*, *pr*, *rsds* and *elev* as inputs.

Reconstructed MI values for each geological period were subsequently corrected for the physiological effects of past atmospheric CO_2 concentration, following the methodology proposed by Prentice *et al.* (see ref. [79] for details). This correction is essential because conventional climatic moisture indices do not correctly represent the environment as experienced by plants. These indices do not account for how atmospheric CO_2 concentration modulates plant water-use efficiency via the stomatal regulation of carbon uptake and water loss[79–82]. For instance, during low-CO_2 periods such as glacial intervals, plants must increase stomatal conductance to acquire sufficient carbon, which increases transpirational water loss[79–82]. The core principle is expressed by the equation[79]:

$$e(T_1, MI_1, c_{a1}) = e(T_0, MI_0, c_{a0}) \quad (3)$$

where e is the ratio of stomatal water loss to carbon uptake; T_1 (°C) is the past growing-season mean temperature; MI_1 (unitless) is the 'true' past value of MI (to be estimated); c_{a1} (ppm) is the past ambient CO_2 concentration; T_0 (°C) is the recent growing-season mean temperature; MI_0 (unitless) is the reconstructed past value of MI; and c_{a0} (ppm) is the recent ambient CO_2 concentration.

We used climatological data for the period 1981–2010 as a reference. For the reference period and the six representative geological periods, we calculated the mean growing-season temperature,

456 defined as the average temperature during days of a year with climatological temperatures above
457 0 °C. We also reconstructed the MI for all periods using the SPLASH model and Eq. (2). The *tas*, *pr*
458 and *rsds* of the reference period were obtained from CHELSA V2.1 (https://chelsa-climate.org/)[83],
459 at a spatial resolution of 30 arc-seconds (*ca*. 0.01°). Global elevation data for the reference period
460 (*elev*, m) were acquired from WorldClim v.2.1 (https://www.worldclim.org/)[74], also at 30
461 arc-seconds. Global atmospheric CO_2 concentration data for the reference period (1981–2010) and
462 for the pre-industrial (pre-1850) and recent (1901–1989) periods, were downloaded from NOAA
463 (https://doi.org/10.15138/9N0H-ZH07)[84]. For the Eocene, average atmospheric CO_2 concentration
464 was derived from refs. [85] and [86]. The Mid-Pliocene CO_2 concentration was obtained from refs. [87]
465 and [88], the LGM CO_2 concentration was acquired from ref. [89], and the Mid-Holocene CO_2
466 concentration was downloaded from NOAA Paleoclimatology Data[90]. All raster data were rescaled
467 to a uniform spatial resolution of 1° using the 'projectRaster()' function in the R package *raster*[76].
468 We then applied 'corrected_mi()' function in the R package *codos*[91], which implements the equation
469 of Prentice *et al*.[79], to correct MI values for the selected six geological periods. All data
470 manipulations and the following analyses were conducted in R v4.3.2 (https://www.r-project.org/)[92].

471 **Quantification of spatio-temporal climate dynamics**

472 A two-dimensional climatic space was defined using recent T_m and ln MI data from 1901 to 1989.
473 This period was chosen to reflect baseline climatic conditions after industrialisation but before the
474 rapid anthropogenic influence – such as accelerated greenhouse gas emissions and a step-up in
475 warming rate – that began around 1990[47]. The climatic space was constructed at multiple
476 resolutions by dividing each axis into 30, 40, 50 or 60 equal intervals. Resolutions below 30
477 intervals yielded insufficient data for robust analysis, while those exceeding 60 intervals provided
478 no substantial increase in sample size. Analyses were performed across all resolutions. Results
479 based on the 30-interval climatic space are presented in the main text, with results from other
480 resolutions detailed in the Supplementary Information.

481 The climatic space was discretised into a grid of 'climatic bins', each representing a unique
482 recent climatic condition. The geographic distribution of each of these climatic conditions was then
483 identified across all six geological periods. Specifically, for each period, we determined the set of

484 geographic grid cells in the geographic space that correspond to each climatic bin in the climatic
485 space – that is, all geographic locations sharing the same climatic conditions.
486 To characterise the deep-time geographic dynamics of climate, we defined and calculated five
487 metrics. First, we identified the earliest occurrence of each climatic condition across the six
488 geological periods, referred to as its 'Age'. We then counted the number of periods in which each
489 climatic condition was present across all six periods. This metric was termed 'Persistence'. The
490 geographic extent of each climatic condition within a given period was measured as the total land
491 surface area it occupied, referred to as 'Area' (Fig. S9). The remaining two metrics quantified
492 changes in the geographic distribution of each climatic condition between the period of its first
493 occurrence (as defined by the metric 'Age') and the recent period. The first, 'ΔArea' (Fig. S10),
494 represents the change in land area occupied by a given climatic condition. Positive values of ΔArea
495 indicate geographic expansion, while negative values indicate contraction. The second metric,
496 'Movement' (Fig. S11), denotes the average geographic shift of a climatic condition between its
497 earliest appearance (Age) and the recent period, calculated using great-circle distances.

498 **Species distribution data**

499 We compiled occurrence records for each vascular plant species based on the accepted species
500 listed in the World Checklist of Vascular Plants (WCVP)[49] from six openly accessible databases: (1)
501 Global Biodiversity Information Facility (GBIF, https://www.gbif.org; accessed in Feb–June 2024)
502 using the R package *rgbif*[93]; (2) Botanical information and Ecology Network (BIEN version 4.2,
503 https://bien.nceas.ucsb.edu/bien/; accessed in Feb–March 2024) using the R package *BIEN*[94,95]; (3)
504 Atlas of Living Australia (ALA, https://www.ala.org.au/; accessed in Feb–March 2024); (4)
505 RAINBIO, a mega-database of tropical African vascular plants distributions
506 (https://gdauby.github.io/rainbio/index.html; accessed in Feb–March 2024)[96]; (5) Flora of Russia
507 (FoR, https://zenodo.org/records/4061848; accessed in Feb–March 2024)[97]; and also (6) WCVP
508 (accessed in Feb–June 2024)[49]. The scientific names of species across all databases were
509 standardised and aligned to the accepted species names in the WCVP before integration.

We subsequently cleaned the species occurrence data using the R packages *dplyr*[98] and *CoordinateCleaner*[99], removing unreliable and non-native data points according to the following process:

(1) Records with erroneous coordinates were excluded, including: no latitude or longitude record, coordinates equal to 0, identical latitude and longitude values, or coordinates falling outside the valid geographic range.

(2) Records with unsuitable data sources, particularly fossil records, were removed, retaining only data points where the 'basis of record' was an observation or preserved specimen.

(3) Records flagged as 'managed', 'introduced', 'invasive' or 'naturalised' in the 'establishment means' field were discarded. Additionally, non-native data points were removed according to the native distribution ranges provided by the WCVP.

(4) Records dated during or before 1945 were excluded, as these older records are generally considered less reliable[100].

(5) Records with 'coordinate uncertainty' greater than 100 km or 'coordinate precision' less than 0.01 were removed.

(6) Records with suspicious 'individual counts' were discarded, retaining records with 0 < 'individual counts' ≤ 100.

(7) The automatic cleaning algorithm by the 'clean_coordinates()' function in the *CoordinateCleaner* R package[99] was run to flag and delete error data points, including: sea coordinates, zero coordinates, mismatched countries, coordinates assigned to country and province centroids, coordinates within city areas, outlier coordinates, and coordinates assigned to biodiversity institutions.

Occurrence records for the same species across different databases were merged. After data cleaning, we retained native occurrence records for 350,864 unique species, representing over 98% of the 357,347 accepted species listed in the WCVP (accessed on 19 February 2024).

Vascular plant diversity

Following the IUCN Red List of Categories and Criteria[101–103], we calculated the extent of occurrence (EOO) for species with ≥3 occurrence records by constructing the minimum convex

polygon encompassing all recorded locations. Portions of the polygons falling outside the native distribution range, as provided by the WCVP, were cropped and excluded. For species with < 3 occurrence records (2,527 species in total), for which EEO could not be calculated, we measured the area of occupancy (AOO), defined as all geographic grid cells at a specific spatial resolution that contain the species' occurrence records[101–103]. In this study, occurrence data were gridded at 1° spatial resolution to estimate AOO. We then created presence-absence raster data at a 1° resolution from the EOO or AOO of each species, with a value of 1 denoting presence (i.e. EOO or AOO) and 0 denoting absence. By stacking the resulting rasters of all species, we produced a global map of land vascular plant species richness. Regions where species richness exceeded the global 90th percentile were defined as plant diversity hotspots[50] (Fig. S3).

Based on the EOO and AOO of each species, we identified the climatic conditions in which each species occurs and generated corresponding presence-absence raster in climatic space. By stacking these rasters, we counted the number of species present in each climatic bin, thereby mapping plant species richness in climatic space (Fig. S4).

The species-level presence-absence data in climatic space were also used to compute multi-site β-diversity within each climatic bin by 'beta.multi()' function in the *betapart* R package[104]. This function calculates the turnover component of β-diversity (Fig. S5) based on the Simpson dissimilarity index, which reflects the degree of species composition turnover among geographic grid cells sharing the same climatic conditions.

To evaluate phylogenetic diversity in climatic space, we constructed a time-calibrated phylogenetic tree for all 350,864 vascular plant species. The initial tree was generated using the 'phylo.maker' function in the *V.PhyloMaker2* R package[105]. The backbone for this tree was the GBOTB.extended megatree, a time-calibrated phylogeny of vascular plants that integrates the Smith and Brown's phylogeny of seed plants[106] and Zanne *et al.*'s plant phylogeny including pteridophyte species[107]. Species absent from the megatree were grafted onto this backbone using a hierarchical approach that places species at the basal node of their genus or, if the genus is missing, at a calculated position within their family[105,108]. This resulting phylogeny, comprising 350,705 successfully placed tips, was then completed to cover all 350,864 species using the 'phylo.maker' function from the *U.PhyloMaker* R package[108].

Based on the comprehensive phylogeny of vascular plants, two phylogenetic diversity metrics were calculated. First, we calculated Faith's phylogenetic diversity (PD, Ma)[57] for each climatic bin, defined as the total branch length of the minimum phylogenetic subtree connecting all species present in that bin (Fig. S6). Higher PD values thus represent greater accumulation of evolutionary history within the climatic bin. To account for the strong, intrinsic correlation between PD and species richness, we also calculated relative phylogenetic diversity (RPD, Ma)[109,110]. RPD was defined as the residuals from an ordinary least squares (OLS) regression of PD against species richness across all climatic bins (Fig. S7). Higher positive RPD values therefore indicate that species in a climatic bin are more phylogenetically overdispersed than expected given their richness (i.e. species are more distantly related and/or more evolutionarily ancient than expected), whereas negative values indicate phylogenetic clustering (i.e. more closely related and/or evolutionarily younger than expected).

Statistical analysis

We first assessed whether recent plant diversity in climatic bins was associated with the earliest occurrence (Age) and temporal persistence (Persistence) of climatic conditions. These relationships were tested using the Kruskal-Wallis test, implemented with the 'kruskal.test()' function in the R *stats* package[92].

The effects of climate and its deep-time geographic dynamics on plant diversity were characterised and visualised using Generalised Additive Models (GAMs) fitted in climatic space. All GAMs excluded interaction terms and employed restricted maximum likelihood (RMEL) to estimate smoothing parameters. Model fitting was performed using the 'gam()' function in the R package *mgcv*[111,112]. Concurvity among explanatory variables was examined prior to model fitting and found to be relatively low (Fig. S12 and Tables S3–S9, S13–S16 and S20–S31).

To estimate the relative contribution of each explanatory variable, we partitioned the total explained deviance into additive components following an approach conceptually analogous to the Lindeman-Merenda-Gold (LMG) method[113]. The relative importance of each variable was calculated as the average of its individual contributions across all possible orderings of variable inclusion.

To test whether climates that were more geographically extensive in the past support greater present-day species richness, we fitted Poisson-distributed GAMs separately for each of the six selected geological periods. In these models, species richness was the response variable, and three explanatory variables were included: two bioclimatic variables (T_m and ln MI), and the geographic extent of each climatic condition (Area) during the corresponding period. In addition, we calculated the mean Area across all periods from the emergence of each climatic condition onward and included it in a separate model. We created contour plots to visualise the relationship between species richness and three explanatory variables. The response surfaces of species richness resulting from the Poisson GAMs were presented as contours in the three-variable space in the form of two-dimensional slices. Convex hulls generated by 'convhulln()' function in the R package *geometry*[114] were applied to avoid representing parts of the fitted surface that are not constrained by data.

To characterise the relationship between plant diversity and the persistence and shifts of climate's geographic extent, we fitted a second set of GAMs. Response variables included species richness, species turnover, and two phylogenetic diversity metrics. Explanatory variables included T_m, ln MI, and Area during the recent period, as well as the ΔArea and Movement of each climatic condition from its first appearance to the recent period. Poisson GAMs were used for species richness, while beta-distributed GAMs with a logit link were used for species turnover, which is ranged between 0 and 1. To test the consistency of these relationships across climate Age groups, we grouped climatic bins by Age and fitted the same GAM structure within each group. Groups postdating the Mid-Holocene were excluded due to insufficient sample size. Partial residual plots were used to visualise the independent relationships between each explanatory variable and each diversity metric. Relative variable importance was calculated as described above.

To test for robustness across modelling approaches, we also fitted Generalised Linear Models (GLMs) with the same response and explanatory variables as the GAMs (Tables S11, S12, S18 and S19). Additionally, we fitted quadratic GLMs incorporating second-order polynomial terms to account for potential non-linear effects. All GLMs were implemented using the 'glm()' function in the *stats* R package[92].

We assessed potential spatial autocorrelation in our analyses, which typically leads to an overestimation of the significance and coefficient estimates of explanatory variables, thereby introducing bias. We performed Moran's *I* test on the residuals of all models using the 'moran.test()' function in the *spdep* R package[115]. All *Moran's I* values were low and/or not statistically significant (Tables S32–S36), suggesting that model results are robust to spatial structure in the data.

Data availability

All climate, palaeoclimate, and species distribution data used in this study are publicly accessible, with full details of data sources and processing described in the Methods. All other data required to reproduce the analyses of this study are available at: https://zenodo.org/records/17743541?token=eyJhbGciOiJIUzUxMiJ9.eyJpZCI6IjFiNDgyOWQ3LTcxODMtNDVkOS04NzZiLWQ2YWNjYTM4ODFjMyIsImRhdGEiOnt9LCJyYW5kb20iOiJiOGQ4ZjQ3YWRhZGNlNTM5NjE5NTBjYjk5NzUzMTUxZiJ9.-nvTzYwNB1lhSrQbXjRnr4uIMp2V0mgjTYXtUARgXy4mFS8ejRLWuCIW-XYYss9sg4bzz7y-icX_t3vBuLgH5Q (private link for Peer Review).

Code availability

The reproducible R Scripts used to conduct all data manipulations and analyses are available at: https://zenodo.org/records/17743541?token=eyJhbGciOiJIUzUxMiJ9.eyJpZCI6IjFiNDgyOWQ3LTcxODMtNDVkOS04NzZiLWQ2YWNjYTM4ODFjMyIsImRhdGEiOnt9LCJyYW5kb20iOiJiOGQ4ZjQ3YWRhZGNlNTM5NjE5NTBjYjk5NzUzMTUxZiJ9.-nvTzYwNB1lhSrQbXjRnr4uIMp2V0mgjTYXtUARgXy4mFS8ejRLWuCIW-XYYss9sg4bzz7y-icX_t3vBuLgH5Q (private link for Peer Review).

Acknowledgements

J.L. was funded by the scholarship granted by the China Scholarship Council (CSC No. 202108060263).

Author information

Authors and Affiliations

Georgina Mace Centre for the Living Planet, Department of Life Sciences, Imperial College London, Silwood Park Campus, Buckhurst Road, Ascot, SL5 7PY, UK

Jiaze Li & Iain Colin Prentice

Department of Earth System Science, Ministry of Education Key Laboratory for Earth System Modeling, Institute for Global Change Studies, Tsinghua University, Beijing 100084, China

Iain Colin Prentice

Contributions

J.L. and I.C.P. conceived the study. J.L. developed the methods, performed data collection and manipulation, carried out all analyses and visualisations, and drafted the manuscript under the supervision of I.C.P. J.L. and I.C.P. revised the manuscript.

Corresponding author

Correspondence to Jiaze Li (email: jiaze.li19@imperial.ac.uk).

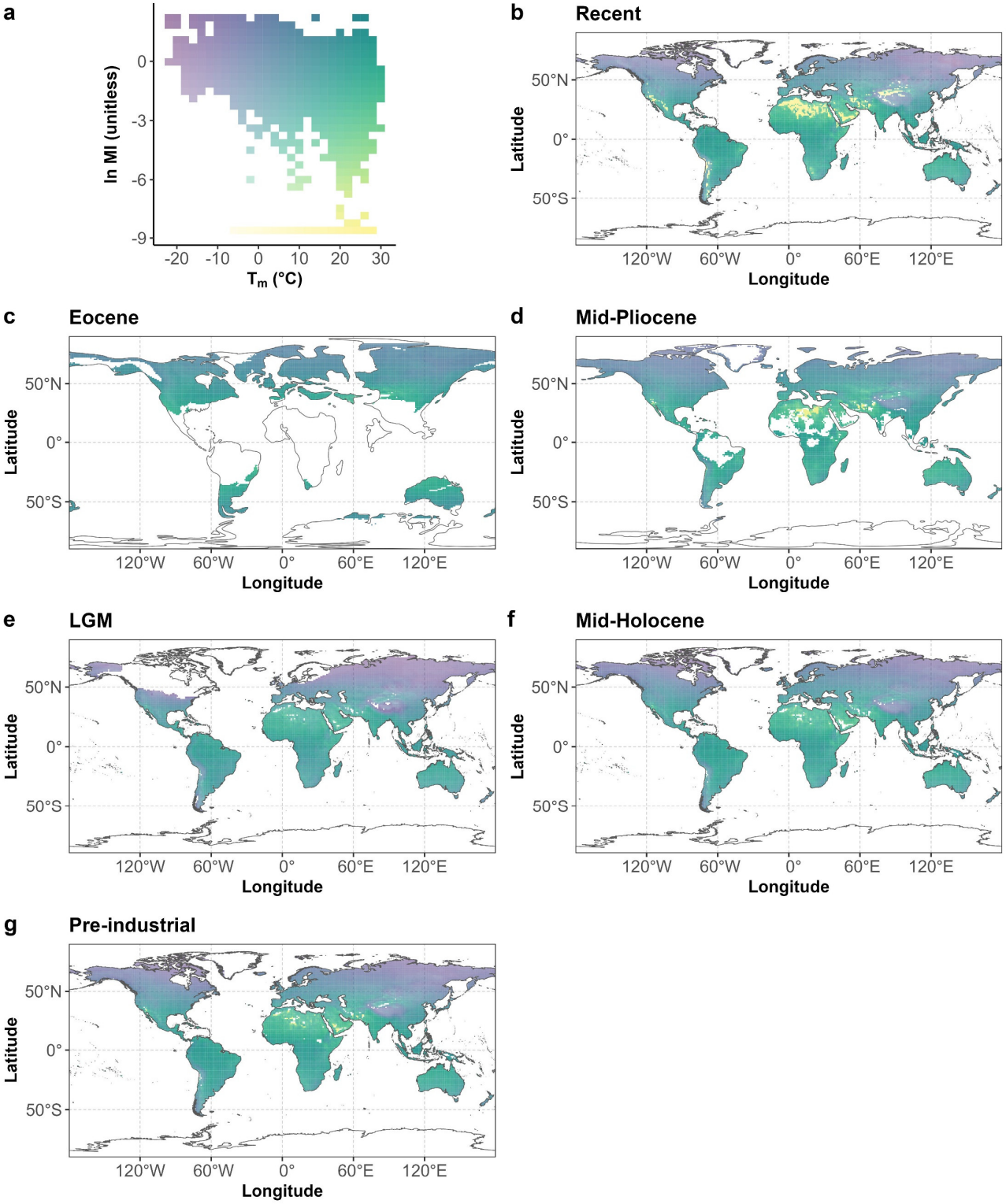
Ethics declarations

Competing interests

The authors declare no competing interests.

Extended data figures and tables

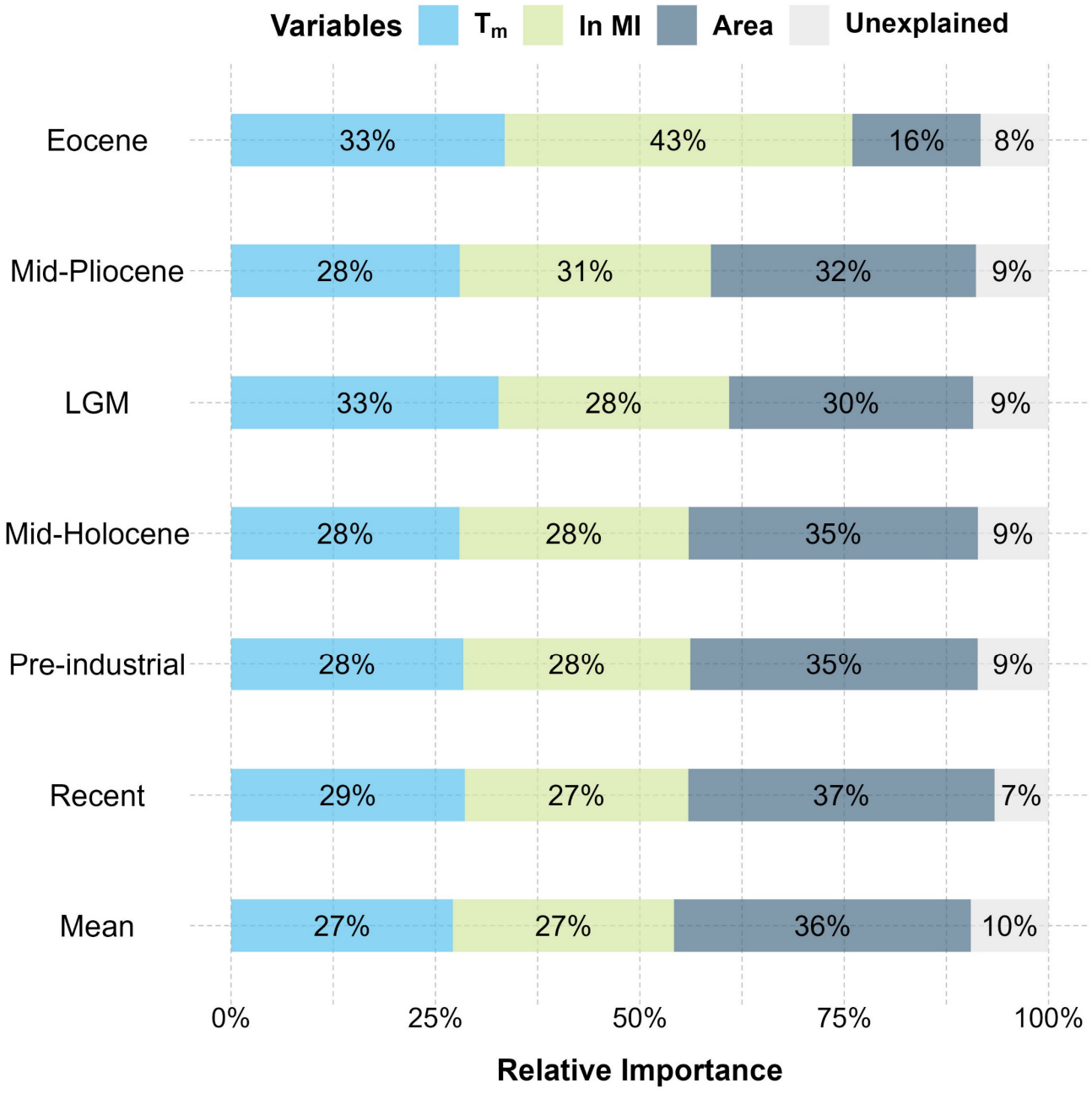
Extended Data Fig. 1 Historical geography of recent climates.



a, The two-dimensional climatic space defined by the recent (1901–1989) climatic conditions (T_m and ln MI), partitioned into 30 equal intervals along each axis. Each coloured grid cell ('climatic bin') represents a unique climatic condition (405 cells in total). Alternative colour gradient schemes are

provided in Figs. S1 and S2. **b**–**g**, Geographic locations where those recent climatic conditions existed during the recent period (1901–1989, **b**), Eocene (*ca.* 50 Ma, **c**), Mid-Pliocene (3.3–3.0 Ma, **d**), Last Glacial Maximum (LGM, 22–18 ka, **e**), Mid-Holocene (*ca.* 6 ka, **f**) and pre-industrial period (pre-1850, **g**). Uncoloured areas denote climatic conditions absent during this period. Colours correspond to those in **a**, with identical colours indicating the same climatic conditions. All maps are shown at a 1° spatial resolution.

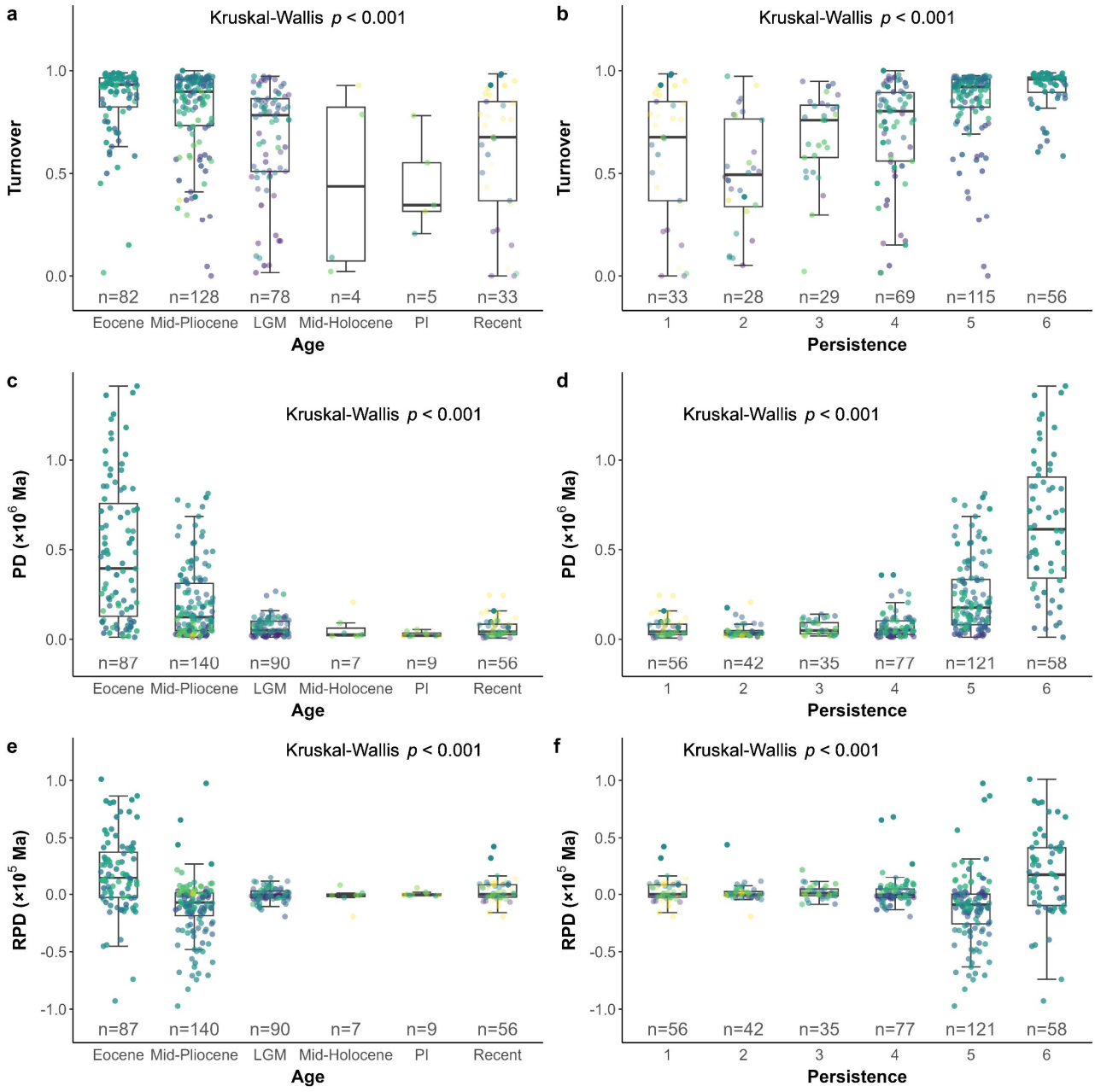
Extended Data Fig. 2 Relative importance of climate and its historical geographic extent in explaining plant species richness.



Relative importance of three explanatory variables estimated by partitioning deviance explained by Generalised Additive Models (GAMs). T_m (°C), recent (1901–1989) temperature index; ln MI (unitless), recent natural-log-transformed moisture index; Area (km^2), total land surface area occupied by each climatic condition during the corresponding geological period. Mean Area since the first appearance of each climatic condition across all selected geological periods was fitted in a separate model. Each stacked bar represents the total deviance in species richness, with coloured

687 segments indicating the proportion attributed to each explanatory variable and the grey segment
688 showing unexplained deviance.

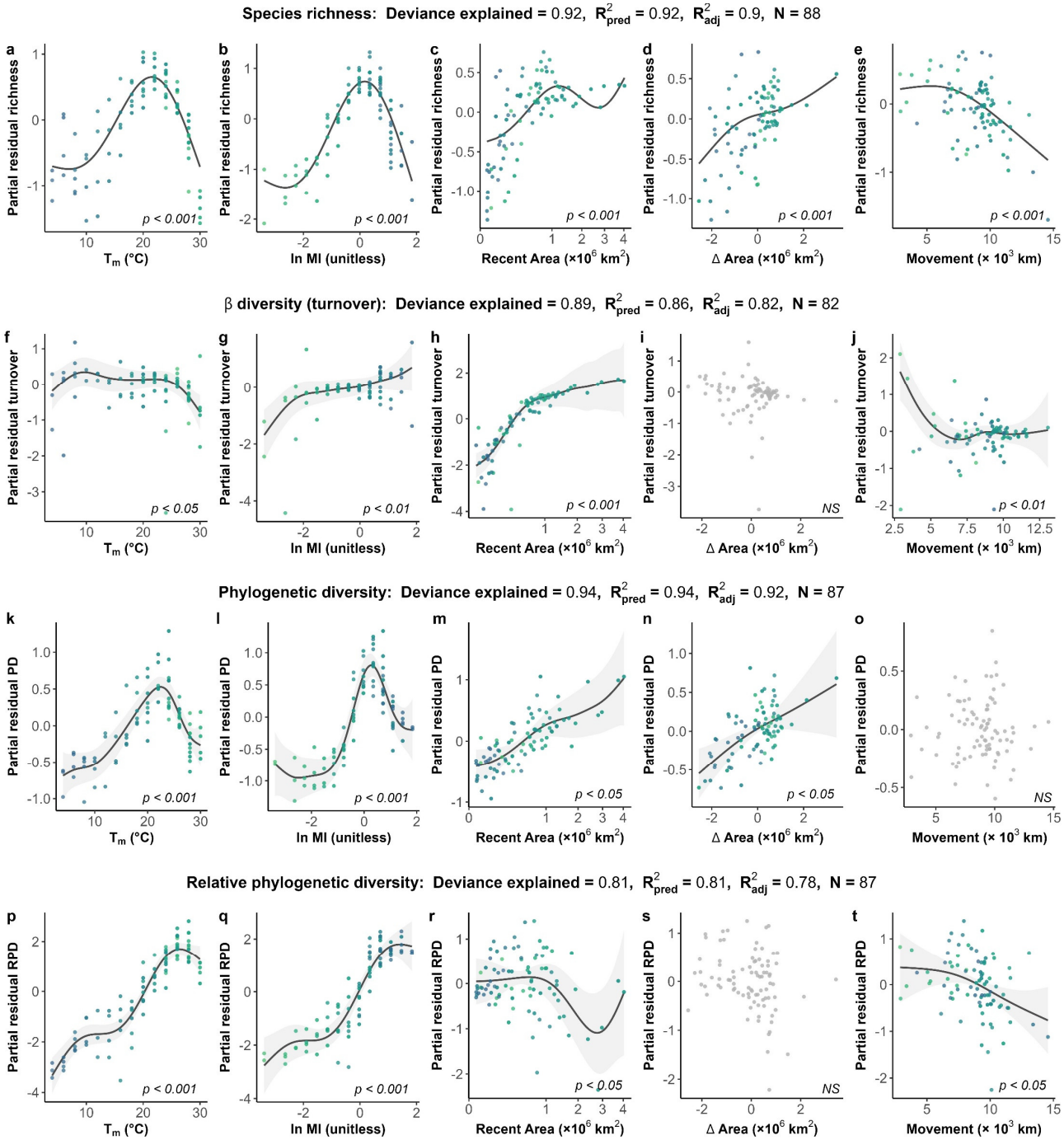
Extended Data Fig. 3 Relationships between recent plant diversity and age or persistence of climate.



a–**b**, Relationships between species turnover and Age (**a**) or Persistence (**b**) of climatic conditions. **c**–**d**, Relationships between Faith's phylogenetic diversity (PD) and Age (**c**) or Persistence (**d**) of climatic conditions. **e**–**f**, Relationships between relative phylogenetic diversity (RPD) and Age (**e**) or Persistence (**f**) of climatic conditions. *p*-values were assessed using Kruskal-Wallis tests. Each coloured dot represents a climatic bin, with colours following the gradient used in **Fig. 1c–e**; horizontal lines and boxes indicate medians and interquartile ranges. Sample sizes per group are

shown below the boxes. T_m (°C), recent (1901–1989) temperature index; ln MI (unitless), recent natural-log-transformed moisture index.

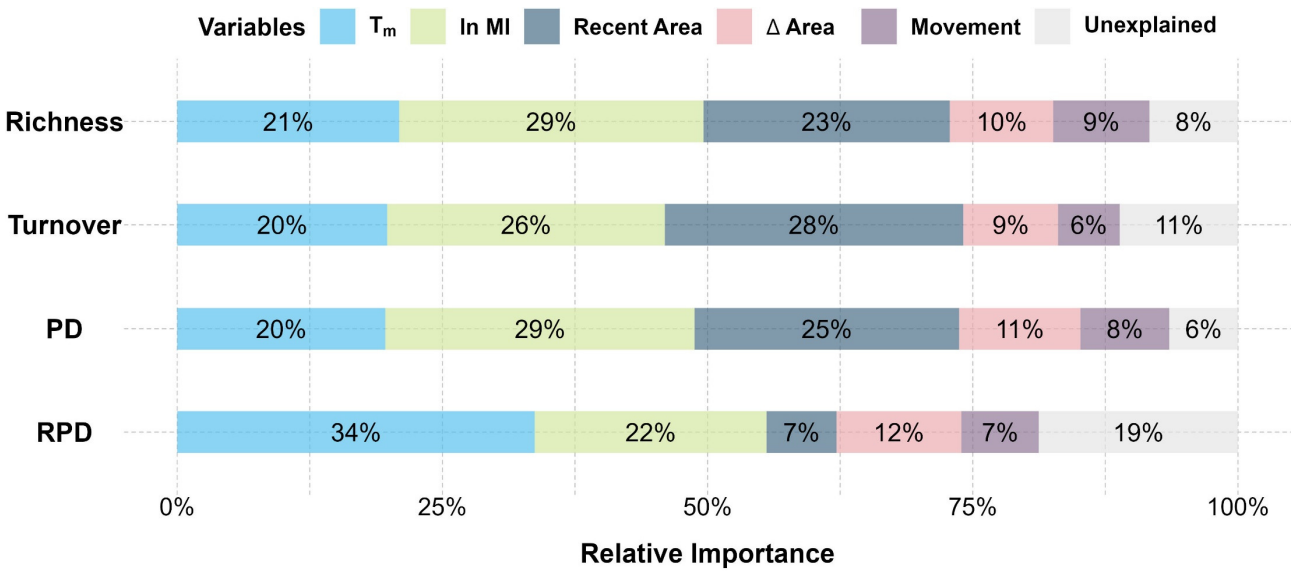
Extended Data Fig. 4 Influence of climatic conditions first occurring in the Eocene (*ca.* 50 Ma) and their deep-time geographic dynamics on plant diversity.



Partial residual plots from Generalised Additive Models (GAMs) showing the independent relationships between four metrics of vascular plant diversity and five explanatory variables. Rows correspond to the four diversity metrics: species richness (**a**–**e**), species turnover (**f**–**j**), phylogenetic diversity (PD, **k**–**o**), and relative phylogenetic diversity (RPD, **p**–**t**). Columns correspond to the five

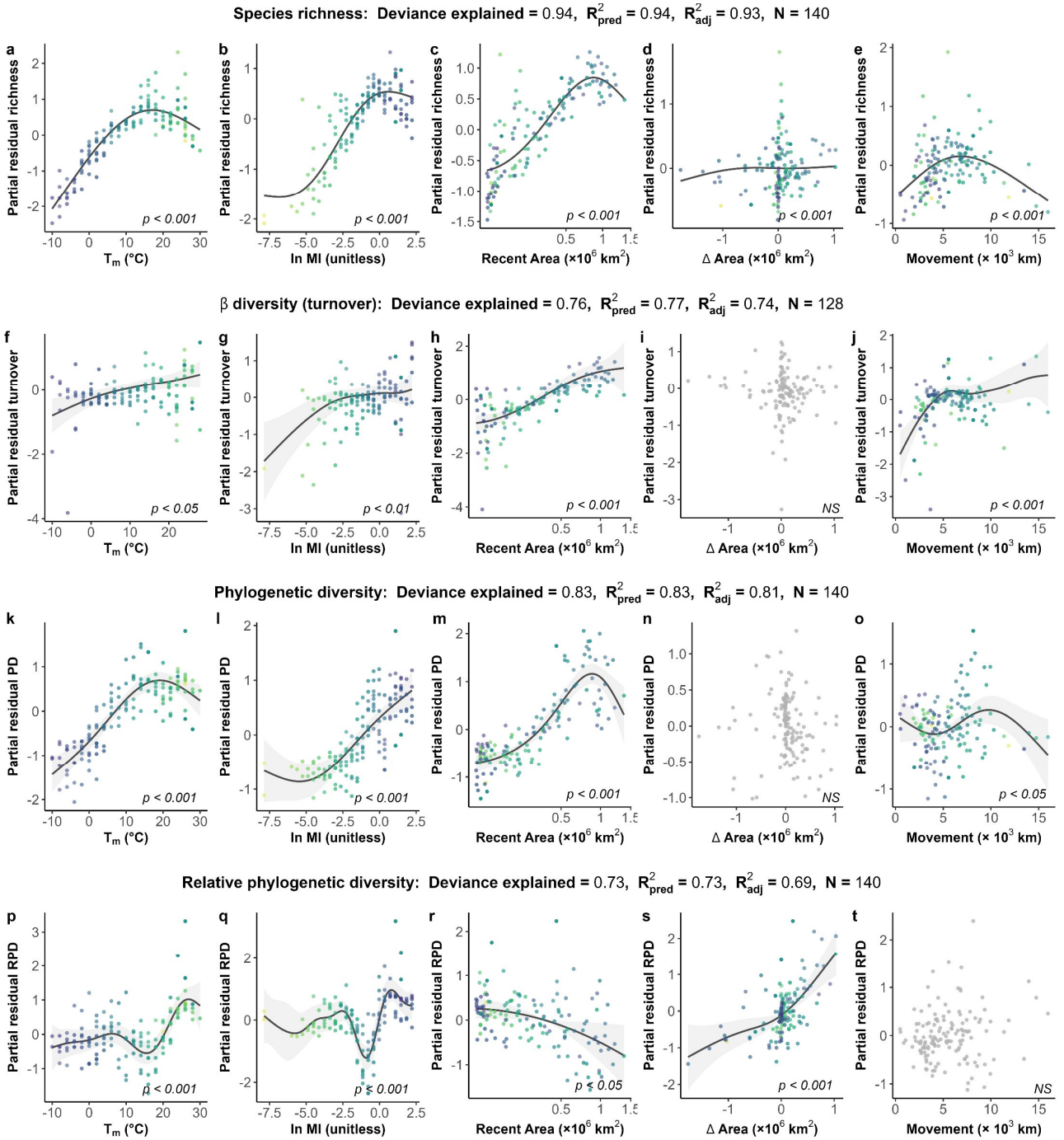
explanatory variables: T_m (°C), recent (1901–1989) temperature index; ln MI (unitless), recent natural-log-transformed moisture index; Recent Area (km^2), total land area occupied by a climatic condition in the recent period; ΔArea (km^2), change in total land area occupied by a climatic condition from its earliest occurrence during the Eocene to the recent period; Movement (km), geographic shift of a climatic condition since its earliest occurrence during the Eocene to the recent period. Black lines represent smooth curves of the GAM regression. Shaded areas indicate 95% confidence intervals, which are not visible in some cases due to narrow uncertainty. Each coloured dot represents a climatic bin, coloured by the gradient used in **Fig. 1c–e**. Statistically non-significant terms ($p > 0.05$) are shown as grey dots with no fitted curve. Model performance is reported as deviance explained, predicted R^2 (R_{pred}^2) and adjusted R^2 (R_{adj}^2).

Extended Data Fig. 5 Relative importance of climate climatic conditions first occurring in the Eocene (*ca.* 50 Ma) and their deep-time geographic dynamics in explaining plant diversity.



Relative importance of five explanatory variables estimated by partitioning deviance explained by Generalised Additive Models (GAMs). T_m (°C), recent (1901–1989) temperature index; ln MI (unitless), recent natural-log-transformed moisture index; Recent Area (km^2), total land area occupied by a climatic condition in the recent period; ΔArea (km^2), change in total land area occupied by a climatic condition from its earliest occurrence during the Eocene to the recent period; Movement (km), geographic shift of a climatic condition since its earliest occurrence during the Eocene to the recent period. Each stacked bar represents the total deviance in a given diversity metric, with coloured segments indicating the proportion attributed to each explanatory variable and the grey segment showing unexplained deviance.

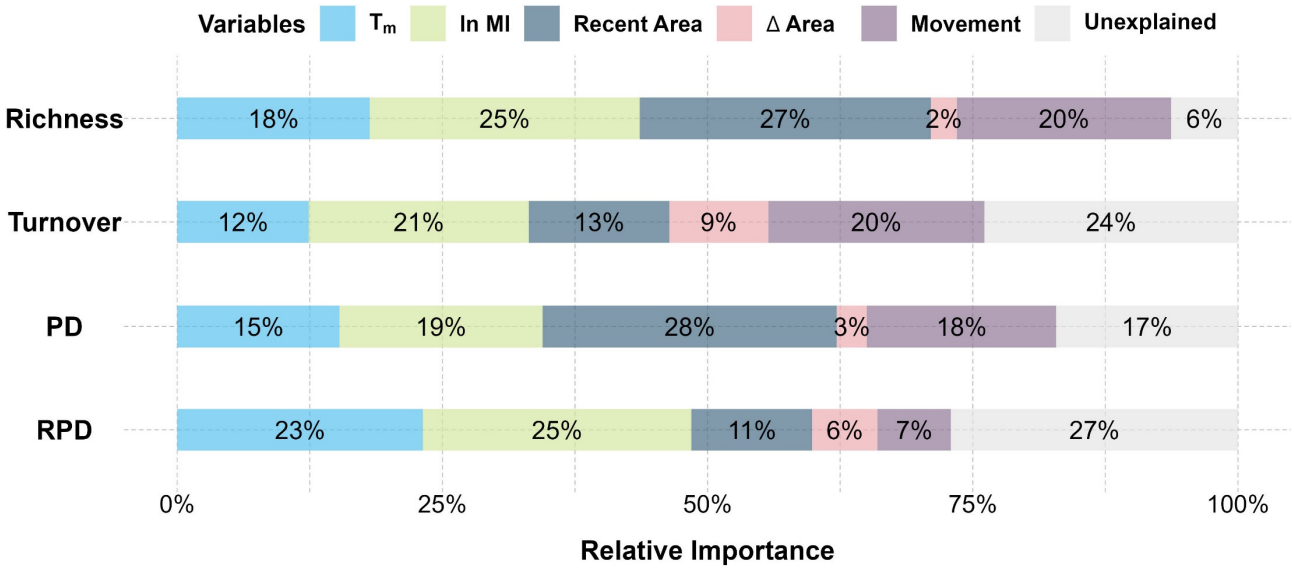
Extended Data Fig. 6 Influence of climatic conditions first occurring in the Mid-Pliocene (3.3–3.0 Ma) and their deep-time geographic dynamics on plant diversity.



Partial residual plots from Generalised Additive Models (GAMs) showing the independent relationships between four metrics of vascular plant diversity and five explanatory variables. Rows correspond to the four diversity metrics: species richness (**a**–**e**), species turnover (**f**–**j**), phylogenetic diversity (PD, **k**–**o**), and relative phylogenetic diversity (RPD, **p**–**t**). Columns correspond to the five

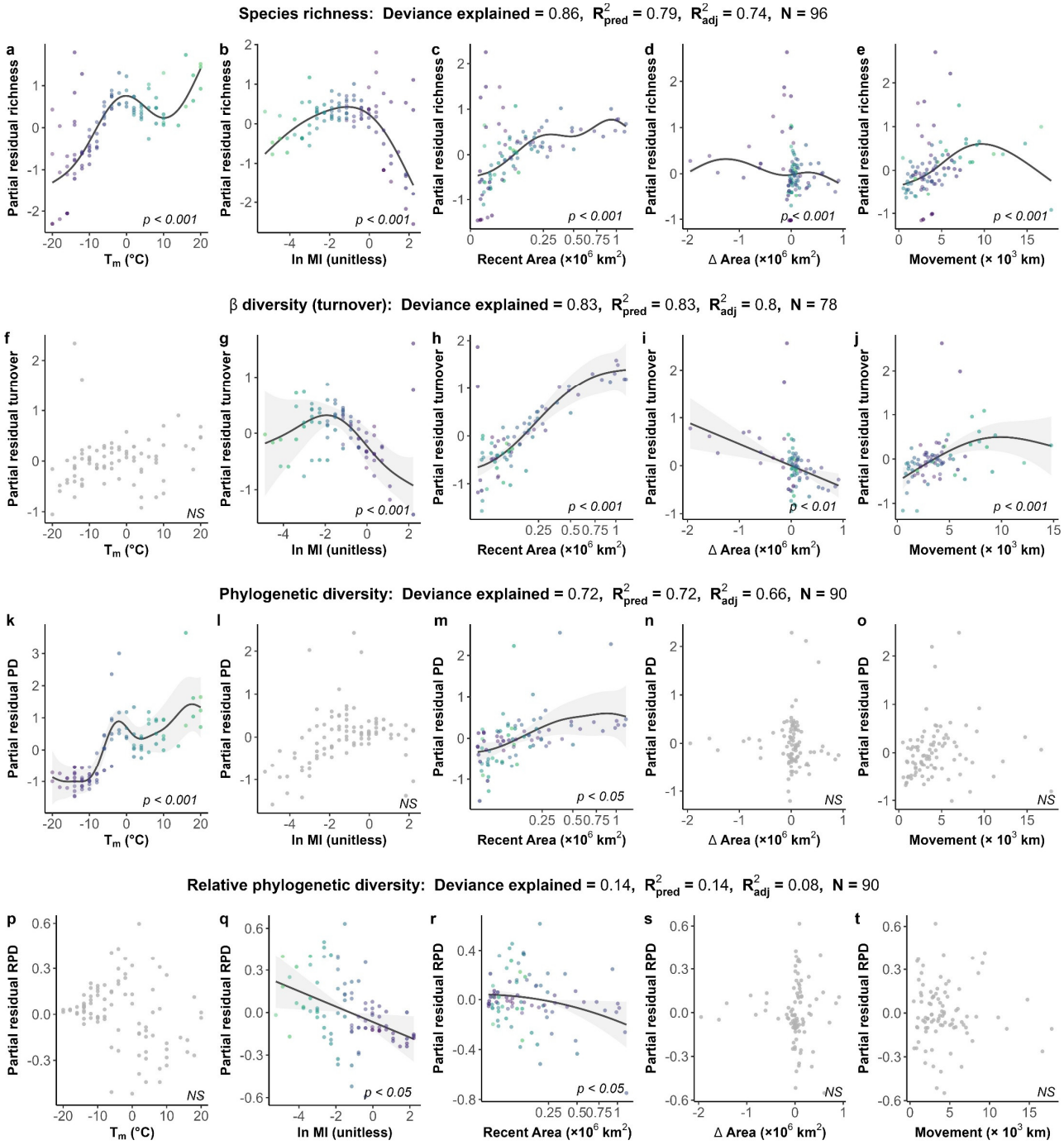
explanatory variables: T_m (°C), recent (1901–1989) temperature index; ln MI (unitless), recent natural-log-transformed moisture index; Recent Area (km^2), total land area occupied by a climatic condition in the recent period; ΔArea (km^2), change in total land area occupied by a climatic condition from its earliest occurrence during the Mid-Pliocene to the recent period; Movement (km), geographic shift of a climatic condition since its earliest occurrence during the Mid-Pliocene to the recent period. Black lines represent smooth curves of the GAM regression. Shaded areas indicate 95% confidence intervals, which are not visible in some cases due to narrow uncertainty. Each coloured dot represents a climatic bin, coloured by the gradient used in **Fig. 1c–e**. Statistically non-significant terms ($p > 0.05$) are shown as grey dots with no fitted curve. Model performance is reported as deviance explained, predicted R^2 (R_{pred}^2) and adjusted R^2 (R_{adj}^2).

Extended Data Fig. 7 Relative importance of climate climatic conditions first occurring in the Mid-Pliocene (3.3–3.0 Ma) and their deep-time geographic dynamics in explaining plant diversity.



Relative importance of five explanatory variables estimated by partitioning deviance explained by Generalised Additive Models (GAMs). T_m (°C), recent (1901–1989) temperature index; ln MI (unitless), recent natural-log-transformed moisture index; Recent Area (km^2), total land area occupied by a climatic condition in the recent period; ΔArea (km^2), change in total land area occupied by a climatic condition from its earliest occurrence during the Mid-Pliocene to the recent period; Movement (km), geographic shift of a climatic condition since its earliest occurrence during the Mid-Pliocene to the recent period. Each stacked bar represents the total deviance in a given diversity metric, with coloured segments indicating the proportion attributed to each explanatory variable and the grey segment showing unexplained deviance.

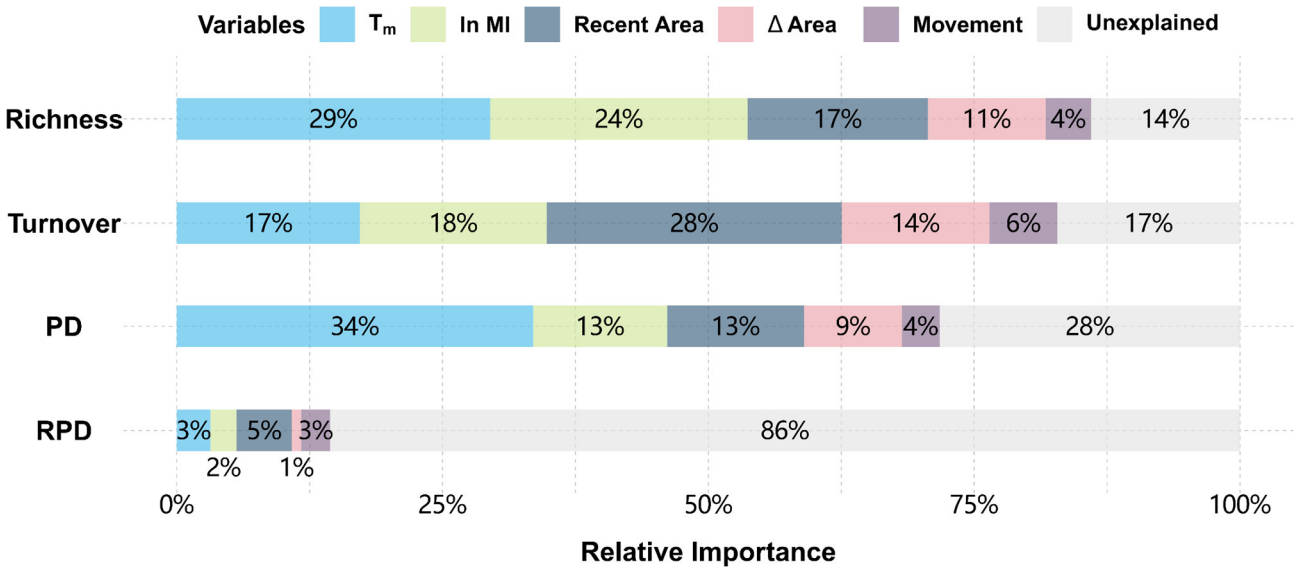
Extended Data Fig. 8 Influence of climatic conditions first occurring in the Last Glacial Maximum (LGM, 22–18 ka) and their deep-time geographic dynamics on plant diversity.



Partial residual plots from Generalised Additive Models (GAMs) showing the independent relationships between four metrics of vascular plant diversity and five explanatory variables. Rows correspond to the four diversity metrics: species richness (**a**–**e**), species turnover (**f**–**j**), phylogenetic diversity (PD, **k**–**o**), and relative phylogenetic diversity (RPD, **p**–**t**). Columns correspond to the five

766 explanatory variables: T_m (°C), recent (1901–1989) temperature index; ln MI (unitless), recent
767 natural-log-transformed moisture index; Recent Area (km^2), total land area occupied by a climatic
768 condition in the recent period; ΔArea (km^2), change in total land area occupied by a climatic
769 condition from its earliest occurrence during the LGM to the recent period; Movement (km),
770 geographic shift of a climatic condition since its earliest occurrence during the LGM to the recent
771 period. Black lines represent smooth curves of the GAM regression. Shaded areas indicate 95%
772 confidence intervals, which are not visible in some cases due to narrow uncertainty. Each coloured
773 dot represents a climatic bin, coloured by the gradient used in **Fig. 1c–e**. Statistically non-significant
774 terms ($p > 0.05$) are shown as grey dots with no fitted curve. Model performance is reported as
775 deviance explained, predicted R^2 (R_{pred}^2) and adjusted R^2 (R_{adj}^2).

Extended Data Fig. 9 Relative importance of climate climatic conditions first occurring in the Last Glacial Maximum (LGM, 22–18 ka) and their deep-time geographic dynamics in explaining plant diversity.



Relative importance of five explanatory variables estimated by partitioning deviance explained by Generalised Additive Models (GAMs). T_m (°C), recent (1901–1989) temperature index; ln MI (unitless), recent natural-log-transformed moisture index; Recent Area (km^2), total land area occupied by a climatic condition in the recent period; ΔArea (km^2), change in total land area occupied by a climatic condition from its earliest occurrence during the LGM to the recent period; Movement (km), geographic shift of a climatic condition since its earliest occurrence during the LGM to the recent period. Each stacked bar represents the total deviance in a given diversity metric, with coloured segments indicating the proportion attributed to each explanatory variable and the grey segment showing unexplained deviance.

Supplementary information

Supplementary Information

Supplementary Figs., Supplementary Tables and Supplementary References.

Reporting Summary

Peer Review File

References

1. Willig, M. R., Kaufman, D. M. & Stevens, R. D. Latitudinal gradients of biodiversity: pattern, process, scale, and synthesis. *Annu. Rev. Ecol. Evol. Syst.* **34**, 273–309 (2003).
2. Turner, J. R. G. Explaining the global biodiversity gradient: energy, area, history and natural selection. *Basic Appl. Ecol.* **5**, 435–448 (2004).
3. Graham, C. H. *et al.* Biodiversity patterns redefined in environmental space. *Ecol. Lett.* **28**, e70008 (2025).
4. Wiens, J. J. & Donoghue, M. J. The origins of the latitudinal diversity gradient: revisiting the tropical conservatism hypothesis. *J. Biogeogr.* e15172 (2025).
5. Hawkins, B. A. Ecology's oldest pattern? *Trends Ecol. Evol.* **16**, 470 (2001).
6. Forster, J. R. *Observations Made During a Voyage Round the World*. (London, G. Robinson, 1778). doi:https://doi.org/10.5962/bhl.title.50538.
7. Norberg, J., Urban, M. C., Vellend, M., Klausmeier, C. A. & Loeuille, N. Eco-evolutionary responses of biodiversity to climate change. *Nat. Clim. Chang.* **2**, 747–751 (2012).
8. Rangel, T. F. *et al.* Modeling the ecology and evolution of biodiversity: Biogeographical cradles, museums, and graves. *Science.* **361**, eaar5452 (2018).
9. Saupe, E. E. *et al.* Spatio-temporal climate change contributes to latitudinal diversity gradients. *Nat. Ecol. Evol.* **3**, 1419–1429 (2019).
10. Urban, M. C. Climate change extinctions. *Science.* **386**, 1123–1128 (2024).
11. Wiens, J. J. *et al.* Niche conservatism as an emerging principle in ecology and conservation biology. *Ecology Letters* vol. 13 1310–1324 (2010).

12. Brown, S. C., Wigley, T. M. L., Otto-Bliesner, B. L., Rahbek, C. & Fordham, D. A. Persistent Quaternary climate refugia are hospices for biodiversity in the Anthropocene. *Nat. Clim. Chang.* **10**, 244–248 (2020).
13. Coelho, M. T. P. *et al.* The geography of climate and the global patterns of species diversity. *Nature* **622**, 537–544 (2023).
14. Kreft, H. & Jetz, W. Global patterns and determinants of vascular plant diversity. *Proc. Natl. Acad. Sci.* **104**, 5925–5930 (2007).
15. Tordoni, E., Carmona, C. P., Toussaint, A., Tamme, R. & Pärtel, M. Global patterns and determinants of multiple facets of plant diversity. *Glob. Ecol. Biogeogr.* **33**, e13823 (2024).
16. Thompson, L. R. *et al.* A communal catalogue reveals Earth's multiscale microbial diversity. *Nature* **551**, 457–463 (2017).
17. Mittelbach, G. G. *et al.* Evolution and the latitudinal diversity gradient: speciation, extinction and biogeography. *Ecol. Lett.* **10**, 315–331 (2007).
18. Fine, P. V. A. Ecological and evolutionary drivers of geographic variation in species diversity. *Annu. Rev. Ecol. Evol. Syst.* **46**, 369–392 (2015).
19. Hutchinson, G. E. Homage to Santa Rosalia or why are there so many kinds of animals? *Am. Nat.* **93**, 145–159 (1959).
20. Wright, D. H. Species-energy theory: an extension of species-area theory. *Oikos* 496–506 (1983).
21. Currie, D. J. Energy and large-scale patterns of animal-and plant-species richness. *Am. Nat.* **137**, 27–49 (1991).
22. Hawkins, B. A. *et al.* Energy, water, and broad-scale geographic patterns of species richness. *Ecology* **84**, 3105–3117 (2003).
23. Evans, K. L., Warren, P. H. & Gaston, K. J. Species–energy relationships at the macroecological scale: a review of the mechanisms. *Biol. Rev.* **80**, 1–25 (2005).
24. Terborgh, J. On the notion of favorableness in plant ecology. *Am. Nat.* **107**, 481–501 (1973).
25. Rosenzweig, M. L. *Species Diversity in Space and Time*. (Cambridge University Press, 1995). doi:https://doi.org/10.1017/CBO9780511623387.

26. Storch, D. & Okie, J. G. The carrying capacity for species richness. *Glob. Ecol. Biogeogr.* **28**, 1519–1532 (2019).
27. Wallace, A. R. *Tropical Nature, and Other Essays*. (Macmillan and Company, 1878).
28. Fischer, A. G. Latitudinal variations in organic diversity. *Evolution (N. Y).* **14**, 64–81 (1960).
29. Wiens, J. J. & Donoghue, M. J. Historical biogeography, ecology and species richness. *Trends Ecol. Evol.* **19**, 639–644 (2004).
30. Hewitt, G. The genetic legacy of the Quaternary ice ages. *Nature* **405**, 907–913 (2000).
31. Sandel, B. *et al.* The influence of Late Quaternary climate-change velocity on species endemism. *Science.* **334**, 660–664 (2011).
32. Meseguer, A. S. & Condamine, F. L. Ancient tropical extinctions at high latitudes contributed to the latitudinal diversity gradient. *Evolution (N. Y).* **74**, 1966–1987 (2020).
33. Davis, M. B. & Shaw, R. G. Range shifts and adaptive responses to Quaternary climate change. *Science.* **292**, 673–679 (2001).
34. Fine, P. V. A. & Ree, R. H. Evidence for a time-integrated species-area effect on the latitudinal gradient in tree diversity. *Am. Nat.* **168**, 796–804 (2006).
35. Bar-On, Y. M., Phillips, R. & Milo, R. The biomass distribution on Earth. *Proc. Natl. Acad. Sci.* **115**, 6506–6511 (2018).
36. Schneider, H. *et al.* Ferns diversified in the shadow of angiosperms. *Nature* **428**, 553–557 (2004).
37. Hughes, C. E., Nyffeler, R. & Linder, H. P. Evolutionary plant radiations: where, when, why and how? *New Phytol.* **207**, 249–253 (2015).
38. Tietje, M. *et al.* Global hotspots of plant phylogenetic diversity. *New Phytol.* **240**, 1636–1646 (2023).
39. Harrison, S. P. *et al.* Paleoclimate Perspectives on Contemporary Climate Change. *Annu. Rev. Environ. Resour.* **50**, (2025).
40. Zuntini, A. R. *et al.* Phylogenomics and the rise of the angiosperms. *Nature* **629**, 843–850 (2024).

41. Gordon, J. D., Fagan, B., Milner, N. & Thomas, C. D. Floristic diversity and its relationships with human land use varied regionally during the Holocene. *Nat. Ecol. Evol.* **8**, 1459–1471 (2024).
42. Woodward, F. I. *Climate and Plant Distribution*. (Cambridge University Press, 1987).
43. Prentice, I. C. *et al.* Special paper: a global biome model based on plant physiology and dominance, soil properties and climate. *J. Biogeogr.* 117–134 (1992).
44. Harrison, S. P. *et al.* Ecophysiological and bioclimatic foundations for a global plant functional classification. *J. Veg. Sci.* **21**, 300–317 (2010).
45. Li, J. & Prentice, I. C. Global patterns of plant functional traits and their relationships to climate. *Commun. Biol.* **7**, 1136 (2024).
46. Ghalambor, C. K., Huey, R. B., Martin, P. R., Tewksbury, J. J. & Wang, G. Are mountain passes higher in the tropics? Janzen's hypothesis revisited. *Integr. Comp. Biol.* **46**, 5–17 (2006).
47. Samset, B. H. *et al.* Steady global surface warming from 1973 to 2022 but increased warming rate after 1990. *Commun. Earth Environ.* **4**, 400 (2023).
48. Colwell, R. K. & Rangel, T. F. Hutchinson's duality: the once and future niche. *Proc. Natl. Acad. Sci.* **106**, 19651–19658 (2009).
49. Govaerts, R., Nic Lughadha, E., Black, N., Turner, R. & Paton, A. The World Checklist of Vascular Plants, a continuously updated resource for exploring global plant diversity. *Sci. data* **8**, 215 (2021).
50. Cai, L. *et al.* Global models and predictions of plant diversity based on advanced machine learning techniques. *New Phytol.* **237**, 1432–1445 (2023).
51. Rafiqpoor, D., Kier, G. & Kreft, H. Global centers of vascular plant diversity. *Nov. Acta Leopoldina NF* **92**, 61–83 (2005).
52. Kier, G. *et al.* Global patterns of plant diversity and floristic knowledge. *J. Biogeogr.* **32**, 1107–1116 (2005).
53. Weigelt, P., König, C. & Kreft, H. GIFT–A global inventory of floras and traits for macroecology and biogeography. *J. Biogeogr.* **47**, 16–43 (2020).

54. Brummitt, N., Araújo, A. C. & Harris, T. Areas of plant diversity—What do we know? *Plants, People, Planet* **3**, 33–44 (2021).
55. Sabatini, F. M. *et al.* Global patterns of vascular plant alpha diversity. *Nat. Commun.* **13**, 4683 (2022).
56. Myers, N., Mittermeier, R. A., Mittermeier, C. G., Da Fonseca, G. A. B. & Kent, J. Biodiversity hotspots for conservation priorities. *Nature* **403**, 853–858 (2000).
57. Faith, D. P. Conservation evaluation and phylogenetic diversity. *Biol. Conserv.* **61**, 1–10 (1992).
58. Cai, L. *et al.* Environmental filtering, not dispersal history, explains global patterns of phylogenetic turnover in seed plants at deep evolutionary timescales. *Nat. Ecol. Evol.* **9**, 314–324 (2025).
59. Stebbins, G. L. *Flowering plants: evolution above the species level*. (Harvard University Press, 1974).
60. Haffer, J. Speciation in Amazonian Forest Birds: Most species probably originated in forest refuges during dry climatic periods. *Science.* **165**, 131–137 (1969).
61. Svenning, J.-C., Eiserhardt, W. L., Normand, S., Ordonez, A. & Sandel, B. The influence of paleoclimate on present-day patterns in biodiversity and ecosystems. *Annu. Rev. Ecol. Evol. Syst.* **46**, 551–572 (2015).
62. Corlett, R. T. & Westcott, D. A. Will plant movements keep up with climate change? *Trends Ecol. Evol.* **28**, 482–488 (2013).
63. Smith, J. *et al.* BioDeepTime: A database of biodiversity time series for modern and fossil assemblages. *Glob. Ecol. Biogeogr.* **32**, 1680–1689 (2023).
64. Cai, L. *et al.* Environmental filtering, not dispersal history, explains global patterns of phylogenetic turnover in seed plants at deep evolutionary timescales. *Nat. Ecol. Evol.* 1–11 (2024).
65. Marder, E., Smiley, T. M., Yanites, B. J. & Kravitz, K. Direct effects of mountain uplift and topography on biodiversity. *Science.* **387**, 1287–1291 (2025).

66. Baste, I. A. & Watson, R. T. *Making peace with nature: a scientific blueprint to tackle the climate, biodiversity and pollution emergencies*. *United Nations Environment Programme (UNEP)* https://www.unep.org/resources/making-peace-nature (2021).
67. United Nations Convention on Biological Diversity. *Biodiversity COP 16: Important Agreement Reached Towards Goal of 'Making Peace with Nature'*. https://www.cbd.int/article/agreement-reached-cop-16 (2024).
68. UN Environment Programme. Kunming-Montreal Global Biodiversity Framework (KM-GBF). in *Fifteenth meeting of the Conference of the Parties to the Convention on Biological Diversity (Part Two) Decision 15/4.* (2022).
69. Lawler, J. J., Gross, J. E., Foden, W. B. & Midgley, G. F. Whole-Earth: A Conservation-Planning Paradigm for a Changing Climate. *Glob. Chang. Biol.* **31**, e70328 (2025).
70. Steinig, S.; Abe-Ouchi, A.; de Boer, A.M.; Chan, W.-L.; Donnadieu, Y.; Hutchinson, D.; Knorr, G.; Ladant, J.-B.; Morozova, P.; Niezgodzki, I.; Poulsen, C.J.; Volodin, E.M.; Zhang, Z.; Zhu, J.; Lunt, D. J. Deep-Time Model Intercomparison Project (DeepMIP) Eocene model data version 1.0. *NERC EDS Cent. Environ. Data Anal.* (2024) doi:10.5285/95aa41439d564756950f89921b6ef215.
71. Kageyama, M. *et al.* PMIP4-CMIP6: the contribution of the Paleoclimate Modelling Intercomparison Project to CMIP6. *Geosci. Model Dev. Discuss.* **11**, 1033–1057 (2018).
72. Eyring, V. *et al.* Overview of the Coupled Model Intercomparison Project Phase 6 (CMIP6) experimental design and organization. *Geosci. Model Dev.* **9**, 1937–1958 (2016).
73. University of East Anglia Climatic Research Unit; Harris, I.C.; Jones, P.D.; Osborn, T. CRU TS4.09: Climatic Research Unit (CRU) Time-Series (TS) version 4.09 of high-resolution gridded data of month-by-month variation in climate (Jan. 1901- Dec. 2024). *NERC EDS Cent. Environ. Data Anal.* (2025).
74. Fick, S. E. & Hijmans, R. J. WorldClim 2: new 1-km spatial resolution climate surfaces for global land areas. *Int. J. Climatol.* **37**, 4302–4315 (2017).
75. Markwick, P. J. The palaeogeographic and palaeoclimatic significance of climate proxies for data-model comparisons. (2007).

953 76. Hijmans, R. J. Geographic Data Analysis and Modeling [R package raster version 3.6-30].
954 (2024).
955 77. Sandoval, D., Prentice, I. C. & Nóbrega, R. L. B. Simple process-led algorithms for
956 simulating habitats (SPLASH v. 2.0): robust calculations of water and energy fluxes. *Geosci.*
957 *Model Dev.* **17**, 4229–4309 (2024).
958 78. Davis, T. W. *et al.* Simple process-led algorithms for simulating habitats (SPLASH v. 1.0):
959 robust indices of radiation, evapotranspiration and plant-available moisture. *Geosci. Model*
960 *Dev.* **10**, 689–708 (2017).
961 79. Prentice, I. C., Villegas-Diaz, R. & Harrison, S. P. Accounting for atmospheric carbon
962 dioxide variations in pollen-based reconstruction of past hydroclimates. *Glob. Planet.*
963 *Change* **211**, 103790 (2022).
964 80. Harrison, S. P. & Prentice, C. I. Climate and CO2 controls on global vegetation distribution
965 at the last glacial maximum: analysis based on palaeovegetation data, biome modelling and
966 palaeoclimate simulations. *Glob. Chang. Biol.* **9**, 983–1004 (2003).
967 81. Bragg, F. J. *et al.* Stable isotope and modelling evidence for CO 2 as a driver of glacial–
968 interglacial vegetation shifts in southern Africa. *Biogeosciences* **10**, 2001–2010 (2013).
969 82. Keenan, T. F. *et al.* Increase in forest water-use efficiency as atmospheric carbon dioxide
970 concentrations rise. *Nature* **499**, 324–327 (2013).
971 83. Karger, D. N. *et al.* Climatologies at high resolution for the earth's land surface areas. *Sci.*
972 *data* **4**, 1–20 (2017).
973 84. Lan, X., Tans, P. and K. W. T. Trends in globally-averaged CO2 determined from NOAA
974 Global Monitoring Laboratory measurements. doi:https://doi.org/10.15138/9N0H-ZH07.
975 85. Lunt, D. J. *et al.* DeepMIP: Model intercomparison of early Eocene climatic optimum
976 (EECO) large-scale climate features and comparison with proxy data. *Clim. Past* **17**, 203–
977 227 (2021).
978 86. Anagnostou, E. *et al.* Changing atmospheric CO2 concentration was the primary driver of
979 early Cenozoic climate. *Nature* **533**, 380–384 (2016).
980 87. Burke, K. D. *et al.* Pliocene and Eocene provide best analogs for near-future climates. *Proc.*
981 *Natl. Acad. Sci.* **115**, 13288–13293 (2018).

982 88. Burton, L. E. *et al.* On the climatic influence of CO 2 forcing in the Pliocene. *Clim. Past* **19**,
983 747–764 (2023).
984 89. Bouttes, N., Paillard, D., Roche, D. M., Brovkin, V. & Bopp, L. Last Glacial Maximum CO2
985 and δ13C successfully reconciled. *Geophys. Res. Lett.* **38**, (2011).
986 90. Bereiter, B. *et al.* Revision of the EPICA Dome C CO2 record from 800 to 600 kyr before
987 present. *Geophys. Res. Lett.* **42**, 542–549 (2015).
988 91. Villegas-Diaz, S. P. H. and I. C. P. and R. codos: CO2 Correction Tools. (2022).
989 92. R Core Team. R: A Language and Environment for Statistical Computing. *R Foundation for*
990 *Statistical Computing, Vienna, Austria.* (2024) doi:https://www.R-project.org/.
991 93. Chamberlain, S. *et al.* rgbif: Interface to the Global Biodiversity Information Facility API.
992 (2024).
993 94. Maitner, B. S. *et al.* The bien r package: A tool to access the Botanical Information and
994 Ecology Network (BIEN) database. *Methods Ecol. Evol.* **9**, 373–379 (2018).
995 95. Maitner, B. BIEN: Tools for Accessing the Botanical Information and Ecology Network
996 Database. *R Package* (2023).
997 96. Dauby, G. *et al.* RAINBIO: a mega-database of tropical African vascular plants distributions.
998 *PhytoKeys* **74**, 1–18 (2016).
999 97. Seregin, A. P. *et al.* ‘ Flora of Russia’ on iNaturalist: a dataset. *Biodivers. Data J.* **8**, e59249
1000 (2020).
1001 98. Wickham, H. *et al.* dplyr: A Grammar of Data Manipulation. (2023).
1002 99. Zizka, A. *et al.* CoordinateCleaner: Standardized cleaning of occurrence records from
1003 biological collection databases. *Methods Ecol. Evol.* **10**, 744–751 (2019).
1004 100. Poppenwimer, T., Mayrose, I. & DeMalach, N. Revising the global biogeography of annual
1005 and perennial plants. *Nature* **624**, 109–114 (2023).
1006 101. Gaston, K. J. & Fuller, R. A. The sizes of species’ geographic ranges. *J. Appl. Ecol.* **46**, 1–9
1007 (2009).
1008 102. Keith, D. A. *et al.* Scientific foundations for an IUCN Red List of Ecosystems. *PLoS One* **8**,
1009 e62111 (2013).

103. Bland, L. M., Keith, D. A., Miller, R. M., Murray, N. J. & Rodríguez, J. P. *Guidelines for the application of IUCN Red List of Ecosystems Categories and Criteria, version 1.1*. *International Union for the Conservation of Nature, Gland, Switzerland* (2017).
104. Baselga, A. & Orme, C. D. L. betapart: an R package for the study of beta diversity. *Methods Ecol. Evol.* **3**, 808–812 (2012).
105. Jin, Y. & Qian, H. V. PhyloMaker2: An updated and enlarged R package that can generate very large phylogenies for vascular plants. *Plant Divers.* **44**, 335–339 (2022).
106. Smith, S. A. & Brown, J. W. Constructing a broadly inclusive seed plant phylogeny. *Am. J. Bot.* **105**, 302–314 (2018).
107. Zanne, A. E. *et al.* Three keys to the radiation of angiosperms into freezing environments. *Nature* **506**, 89–92 (2014).
108. Jin, Y. & Qian, H. U. PhyloMaker: An R package that can generate large phylogenetic trees for plants and animals. *Plant Divers.* **45**, 347–352 (2023).
109. Forest, F. *et al.* Preserving the evolutionary potential of floras in biodiversity hotspots. *Nature* **445**, 757–760 (2007).
110. Davies, T. J. & Buckley, L. B. Phylogenetic diversity as a window into the evolutionary and biogeographic histories of present-day richness gradients for mammals. *Philos. Trans. R. Soc. B Biol. Sci.* **366**, 2414–2425 (2011).
111. Wood, S. N. *Generalized additive models: an introduction with R*. (Chapman and Hall/CRC, 2017). doi:https://doi.org/10.1201/9781315370279.
112. Wood, S. mgcv: Mixed GAM Computation Vehicle with Automatic Smoothness Estimation. (2023) doi:10.32614/CRAN.package.mgcv.
113. Lindeman, R. H., Merenda, P. F. & Gold, R. Z. *Introduction to bivariate and multivariate analysis*. (Glenview, Ill. [etc.] : Scott, Foresman and Comp, 1980).
114. Roussel, J.-R. *et al.* Package 'geometry'. *R package* (2023).
115. Bivand, R. *et al.* spdep: Spatial dependence: weighting schemes, statistics and models. *R package* (2024).

Supplementary Files

This is a list of supplementary files associated with this preprint. Click to download.

- nrreportingsummaryJLICPNature.pdf
- nreditorialpolicychecklistJLICPNature.pdf
- SIJLICPNature.pdf
- nrreportingsummaryJiazeLi.pdf